Use of Salvaged Utility Poles in Roadway Bridges: Time-Dependent Behavior of Composite Wood-Concrete Beams

Nathan J. Miller
Richard M. Gutkowski
Jeno Balogh

Department of Civil & Environmental Engineering
Colorado State University

Don Radford
Department of Mechanical Engineering
Colorado State University

December 2009

Acknowledgements

This report was prepared with funds provided by the U.S. Department of Transportation to the Mountain-Plains Consortium. MPC universities include North Dakota State University, Colorado State University (CSU), University of Wyoming, and University of Utah.

Disclaimer

ABSTRACT

This research study focused on the long-term and repeated load behavior of wood-concrete composite beams in which the wood layer is composed of recycled utility poles. Previous research studies have found this type of a beam to have high efficiency and to be a potentially viable replacement for short span bridges on low traffic roadways. Since both wood and concrete exhibit time-dependent behaviors, it is necessary to examine the effects of sustained and repeated loads on the composite beam. Two lab specimens were utilized to examine these behaviors. A long-term load, estimated to be 11% of the maximum capacity, was applied to the first specimen. Due to the rheological effects of the composite beam, the final deflection of the specimen at a time period of 256 days was 1.75 in., which was more than twice the elastic deflection due to the application of the dead and live loads. In order to predict the time-dependent deflection, an existing finite element program was utilized as well as a simplified evaluation method. It was determined that, with modifications, both methods provide accurate predictions. The other specimen in the study was subjected to repeated loads up to the design service load for 35,000 cycles. It was found that the repeated loading does affect the effective stiffness of the beam as it dropped to 94.6% of the initial value as a result of the 35,000 load cycles. In addition, the time-dependent deflection of the specimens during the 28-day concrete curing period was monitored, and an empirical relationship previously developed for specimens with a different span was successfully modified to predict the deflection of specimens with various spans.

TABLE OF CONTENTS

LIST OF TABLES

LIST OF FIGURES

1. INTRODUCTION

This study focuses on the usage of a wood-concrete composite system for short span bridges, utilizing reclaimed utility poles as the wood layer. A wood-concrete composite bridge poses a viable solution for the replacement of deficient short span rural bridges. Currently, there is a need for improvement to the transportation system as about 27% of the nation's bridges are deemed structurally or functionally deficient according to the American Society of Civil Engineers in their *Infrastructure Report Card 2005*.[1] This potential wood-concrete composite system offers many advantages as a viable alternative to traditional timber or reinforced concrete short span bridges on low traffic roads. A wood-concrete composite system can be more efficient than these traditional types of bridges. A large portion of the concrete in a typical reinforced concrete beam or deck cracks, resulting in essentially all of the tensile stresses being resisted by the steel reinforcement, i.e., the concrete itself is wasteful as it resists little or no load. In a layered wood-concrete composite beam, the cracked concrete is replaced by a layer of wood members. Consequently, the concrete layer resists the compressive stresses, and the wood layer resists the tensile stresses. The wood removes the need for the wasted concrete and eliminates most of the expensive steel reinforcement. The concrete layer provides a large amount of added stiffness to the member and protects the wood layer from moisture and resulting deterioration. The wood may still get wet from a driving rain, but there is little concern for the decay of the wood. As more utility wires are being buried, utility poles that are in good condition are being removed and are available at very low or no cost.

The composite bridge system can be built in place with a minimum of formwork and equipment as the utility poles also serve as the formwork for the concrete layer. The only forms needed are for the sides of the bridge deck. The poles are typically lightweight enough to eliminate some of the heavy equipment needs. Shoring is also not necessary as the poles provide sufficient support to the deck as the concrete cures.[2,3] The system is lighter in weight in comparison to a reinforced concrete system, thus it requires smaller foundations.

This research is part of an ongoing series of studies at Colorado State University (CSU) aimed toward the usage of reclaimed utility poles for the wood layer of a composite wood-concrete longitudinal deck bridge. An approximately 2 ft. wide beam, which is a representative section of the intended bridge system, is the basis of the work. Previously, LeBorgne demonstrated the potential of using utility poles in a timber-concrete composite beam[4,5]. He successfully developed a design procedure and spreadsheet (based on the ACI and NDS design codes) to determine the load capacity. To verify the design method, two full-scale specimens were designed, constructed, and load tested to failure. The results of his experimentation included beams with a service and ultimate capacity as high as 12.22 kips and 37.98 kips, respectively, and a composite efficiency (defined subsequently) as high as 96.4%. In addition to determining the load capacity and efficiency of the specimens, he also developed an empirical formula to model the time-dependent deflection of the specimen during the 28-day curing period of the concrete.

This report details the results of subsequent experimental tests of the long-term and repeated load behavior of two specimens similar to those of LeBorgne, but of different spans. Time-dependent response was studied for the 28-day curing period of the concrete under the dead load of the specimen. Then a live load was applied to the specimen and the time-dependent behavior was observed for 256 days. That behavior was predicted using an existing computational model[6,7]. Also, LeBorgne's empirical equation for predicting creep deflections during the 28-day curing period was extended to predict the 28-day deflection of the specimens in this study. Repeated loads, to the calculated design service level for a modest number of cycles, were applied to one of the beams to observe its behavior. The changing

stiffness of the system was monitored as well as permanent changes in deflection. Due to improvements made to the construction process, it was anticipated that the response of the specimen under such loads would be improved as compared with prior repeated load tests involving wood-concrete specimens constructed with dimension lumber.

2. LITERATURE REVIEW

2.1 Connection Detail

The connection detail (interconnection) between the wood and concrete layers is a critical factor in the effectiveness of wood-concrete composites. There are two extremes to this interconnection. At one extreme ("fully non-composite" behavior), the layers are completely free to move relative to each other horizontally. This results in a large amount of slip between the layers and large deflections. At the other extreme ("fully composite" behavior), there is a complete, perfect bond between the two layers allowing no slip. This results in the stiffest case with the smallest deflections. Actual behavior ("partially composite" behavior) lies between these two extremes. The goal of researchers has been to achieve an interconnection that is as close to the fully composite extreme as possible so as to reduce deflection in the beam as much as possible. "Composite efficiency" is a measure used to quantify how close any interconnection comes to achieving the fully composite extreme.

Pault[8] developed a method for determining the composite efficiency (termed "EFF") as expressed by Equation 2.1. EFF is a ratio that relates the deflection of the actual beam (in the partially composite state) to that of a theoretically fully composite beam and a theoretically completely non-composite beam of the same geometric configuration.

$$EFF = \frac{\Delta_N - \Delta_P}{\Delta_N - \Delta_C} \qquad \text{(Equation 2.1)}$$

where Δ_N = the theoretical non-composite deflection
Δ_P = the actual partially composite deflection
Δ_C = the theoretical fully-composite deflection

The experimental partially composite case provides a deflection between the fully-composite and non-composite case. The efficiency is a ratio that demonstrates how close the partially composite deflection is to the fully composite deflection.

Ceccotti has presented a summary of many different methods of interlayer connection that have been used,[9] see Figure 2.1. Group (a) comprises the least stiff interconnections, being composed of nails or steel bars placed vertically between the wood and concrete layers. Group (d) comprises the stiffest connections which involve a steel lattice or plate running the length of the beam. Groups (b) and (c) include examples of connections that are intermediate to the two extremes.

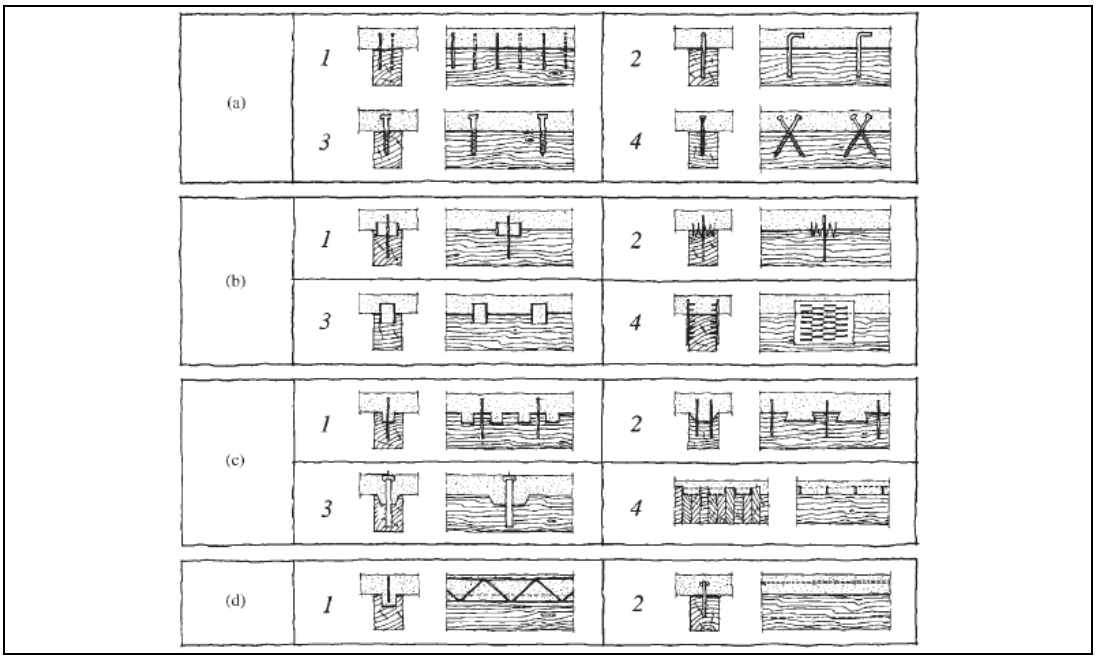

Figure 2.1 Summary of Composite Connections[9]

The interlayer connection detail used in this research is similar to a notched connection developed by Natterer et al[10,11,12] (see Figure 2.2). That connection uses a combination of a notch (shear key) and an anchor between the layers which provides a mechanical interlock between the two layers and resistance to shear and bearing stresses in the notch. The anchor rod that extends through the concrete layer resists the vertical component of the compression force on the side surface of the notch.

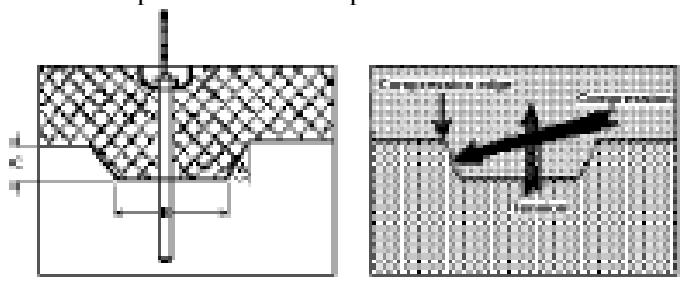

Figure 2.2 Notched Connection Detail[12]

The anchor is a steel dowel that is glued into the wood layer. A plastic sleeve around it prevents the dowel from bonding to the concrete. A nut at the top of the dowel is tightened to provide contact between the two layers. Tightening the anchor partially closes any gap between the concrete and wood resulting from the shrinkage of the concrete and/or any shrinkage or swelling of the wood layer. It is retightened after the concrete cures and can be redone later, if needed, to retighten the system.

Dias indicated that a notched connection should be able to achieve composite efficiencies of approximately 95% if the slip modulus is high.[13] Previous researchers at CSU have used this connection type while studying both beam and deck applications. Brown,[14] Etournaud,[15] Koike,[16] Fast,[2] and To[17] among others physically demonstrated that the connection can achieve a high EFF, but it can vary noticeably. Brown achieved EFF values between 82% and 93.5%. Fast observed EFF values between 40.6% and 69.5%. LeBorgne's[4,5] research included improvements to the notched connection detail, and his two specimens achieved EFF values of 96.4% and 93.6%.

Many numerical models for both the short-term and long-term behavior of wood-concrete composite beams exist. Short-term numerical models include 1D-FEM (Amadio and Fragiacomo[18]), 2-D FEM (Balogh et al.[19]), and 3D-FEM (Kuhlmann and Michelfelder[20]). Long-term numerical models include 1D-FEM developed by Fragiacomo,[6] and 3D-FEM developed by To.[17] The long-term numerical models are described subsequently.

2.2 Concrete Mix Design

Due to the dry climate conditions in Colorado, achieving a quality interface between the concrete and the face of the notch has been challenging. Problems were experienced in the past due to poor consolidation of the concrete in the notches, transverse shrinkage cracks in the concrete, swelling of the wood, and moisture loss of the concrete. Because of the very dry climate, delivered lumber that has been kiln dried to 12% moisture content will continue to dry to an equilibrium point around 6% or 7% moisture content. Consequently, the wood draws moisture from the concrete during curing.

LeBorgne solved the above problems in two steps.[21] First, a waterproofing paint was applied to the timber layer to reduce, if not eliminate, moisture transfer across the timber-concrete interface. This waterproofing paint may not be necessary in all climates. Second, LeBorgne designed (see Table 2.1) a self-leveling concrete with a high slump to improve the consolidation of the concrete in the notch. They had a specified compressive strength of 5 ksi and a slump of 11 in. Supercizer 7 manufactured by Fritz-Pak,[22] a superplasticizer that reduces the water content needed to produce a given slump and reduces the shrinkage of the concrete, was included as an additive.

Table 2.1 LeBorgne Mix Design

Water	389 lbs/yd^3
Type 1 Portland Cement	854 lbs/yd^3
3/8" Course Aggregate	1235 lbs/yd^3
Fine Aggregate with a Fineness Modulus of 2.7	1385 lbs/yd^3
Fritz-Pak Supercizer 7	2.5 lbs/yd^3

Figure 2.3 shows the change in quality of the concrete in the notches as a result of the improved mix design and waterproofing paint.

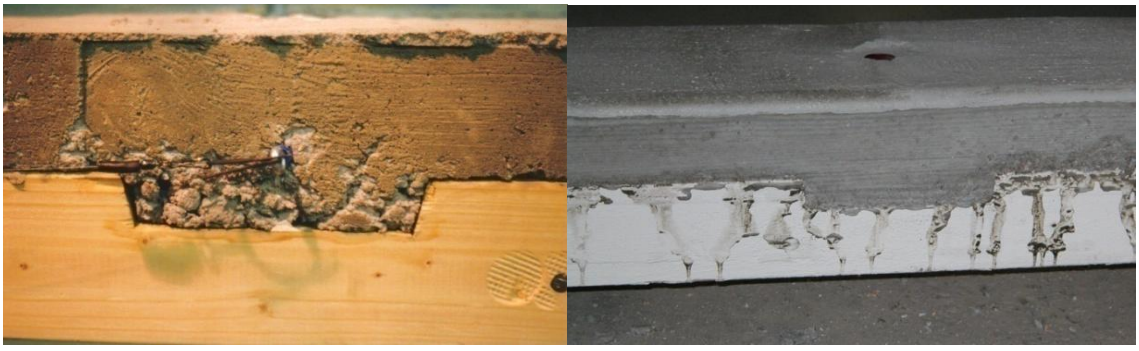

Figure 2.3 Notched Connection (Left–Poor Consolidation, Right–Good Consolidation)

2.3 Previous Load Tests at CSU

MPC-supported research involving the topic of composite wood-concrete longitudinal bridges utilizing round poles for the wood layer is ongoing at CSU. In 2007, LeBorgne[4,5] studied two beams that utilized reclaimed utility poles for the wood layer to confirm a design procedure he developed to determine their service load capacity. That procedure was based on the National Design Specification for Wood Construction[23] and the American Concrete Institute[24] specifications. Two specimens designed using this procedure were then constructed for load testing the reclaimed utility poles obtained from a local utility company as poles that had been removed in a road-widening project.

Construction of the specimens was essentially the same as detailed by LeBorgne.[4,5] The poles were laid with opposite ends next to each other, and the smaller pole at each end of the beam was shimmed up to make a level surface on top. This resulted in a natural camber on the bottom of the beam. After making the notches and placing the dowels, the concrete layer was placed on top of the poles. The interlayer connection is that utilized by Gutkowski et al.,[12] but with some differences (see Figure 2.4). First, the dowel is not protected with a plastic sleeve within the concrete layer. Instead, the concrete is allowed to cure directly around the dowel. The lower length of the dowel extends all the way through a hole in the utility pole, allowing it to be tightened from underneath the poles. This eliminates the need for adhesive between the wood, and the dowel is accessible throughout the life of the bridge. On top of the specimen, an asphalt layer may cover the dowels and limit access to the dowel connection.

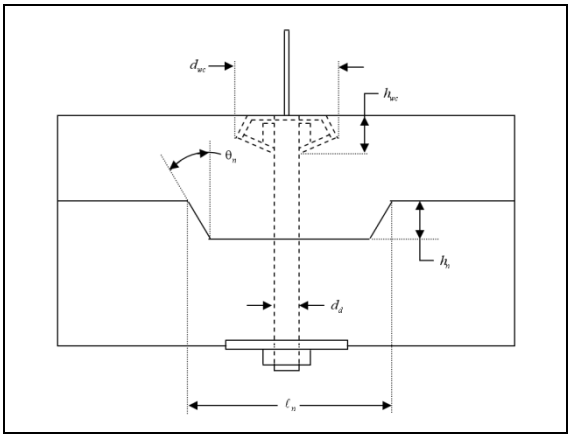

Figure 2.4 LeBorgne Connection Detail[4]

Each of LeBorgne's specimens was two poles wide (as a representative section of the conceived longitudinal deck bridge) and had a span of 354.24 in. Each specimen was load tested under ramp loading with a point load applied at midspan. The failure loads for the specimens were 35.48 kips and 37.98 kips, respectively, and exceeded the calculated design ultimate load values. As stated above, the EFF values were 96.4% and 93.6%, respectively.

2.4 Long-Term Effects

Many complex, time-dependent phenomena are involved in the long-term behavior of wood-concrete composite beams.[2,3] The wood layer experiences creep, mechanosorptive creep, and shrinkage/swelling while the concrete layer experiences creep and shrinkage/swelling. Changes in moisture affect the wood layer, and changes in temperature affect both layers.

Creep is a phenomenon in which a material undergoes increases in strain over time while the applied stress remains constant. Figure 2.5 provides a representation of a generic creep behavior. The plot on the left shows the stress held constant in time, and the plot on the right shows the increasing strain over time.

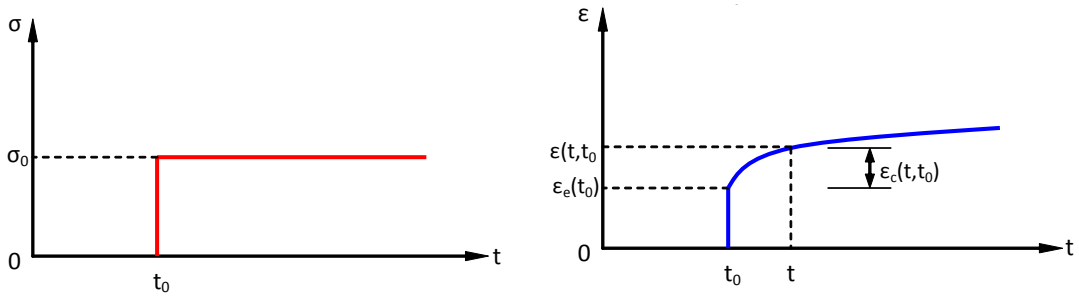

Figure 2.5 Generic Creep Phenomenon[17]

One of the explanations offered by Hanhijärvi[25] for creep in wood is that under a sustained load there is the delayed breaking and reforming of weak hydrogen bonds in the wood. The stronger bonds do not break and contribute to the elastic deflection of wood. Mechanosorptive creep exhibits a similar behavior but is caused by changes in moisture content in the wood. Hanhijärvi says that the sorption of moisture in the wood material can lead to the breaking and reforming of the weak secondary bonds in the structure of the wood.

The creep mechanism in concrete is very complicated. Neville[26] presents several theories and hypotheses regarding the creep mechanisms. In general, the cement paste and the water content of the cement contribute to the creep phenomenon. Shrinkage is also a major contributor to the long-term deflection of concrete. Shrinkage is a phenomenon in which the volume of a concrete section decreases over time separate from any applied load effects.[17] "Drying shrinkage" is dominant and occurs as the water in the concrete evaporates as the concrete cures. "Autogenous shrinkage," which results from chemical reactions taking place in the concrete as it cures, contributes only a small portion of the shrinkage.

In his thesis, Fast experimentally studied the long-term behavior and repeated loading of wood-concrete composite beams.[2,3] The wood layer consisted of nominal 2 in. x 4 in. dimension lumber and used the notched connection described in Figure 2.4. The creep specimens had a span of approximately 140 in. and were loaded to 12.5% of their estimated ultimate load capacity. Eight specimens were allowed to creep for 135 days, and exhibited a range of 53.8% to 60.9% (Avg. = 57.5%) increase in the midspan deflection relative to the initial elastic deflection. The specimen configuration for repeated loading was the same as the creep tests. Eleven specimens were cycled between 700 lb. and 1250 lb. using a sine wave at a frequency of 15 cycles per minute for 21,600 cycles. The average increase in this deflection was 14.2% of the initial deflection under the applied load with a maximum value of 16.4%. The specimens had an average decrease in stiffness of 17.9% with a maximum of 44.1%. The 44.1% loss was an outlier in the data as the second largest decrease in stiffness was approximately 25%. Fast attributed the reduction in specimen stiffness to material degradation and/or interlayer slip along the length of the specimens[2].

The "creep coefficient" is one measure for quantifying the deflection due to creep. Equation 2.2 provides the equation for calculating the total deflection, i.e., including creep.

$$\Delta_T = \Delta_E * (1 + \phi_c) \quad \text{(Equation 2.2)}$$

where Δ_T is the total deflection due to a sustained load, Δ_E is the initial short-term deflection, and ϕ_c is the creep coefficient. The creep coefficient provides the deflection due to creep as a percentage of the elastic deflection of a beam under a sustained load.

2.5 Long-Term Behavior Predictions

The long-term behavior of wood-concrete composites involves the influence of many complex phenomena. The wood layer experiences creep, mechanosorptive creep, shrinkage/swelling, and changing properties with moisture content changes. The concrete layer experiences creep and shrinkage, and the connection experiences creep and mechanosorptive creep over time. All of these phenomena are also affected by changes in the temperature and relative humidity of the surrounding environment.

In order to predict the behavior of a wood-concrete composite beam over time, the contributions due to the above-mentioned phenomena must be considered. Many different models can be used to describe the phenomena. The following describes some of the models that can be utilized to describe the rheological behavior of wood and concrete.

In concrete alone, many models have been used to determine shrinkage and creep. Two of the more common models described here are the ACI 209-82[27] model and the CEB-FIP Model Code 1990.[28] Each model considers the total strain as a linear combination of strains due to creep, strains due to shrinkage, and any strains resulting from an applied load. The equations from each code are shown in Equations 2.3 and 2.4, respectively.[29]

$$Total\ Strain = Shrinkage\ Strain + \frac{Stress}{E_{cmto}} * (1 + Creep\ Coefficient) \quad \text{(Equation 2.3)}$$

$$Total\ Strain = Shrinkage\ Strain + \frac{Stress}{E_{cmto}} + \frac{Stress}{E_{cm28}} * Creep\ Coefficient \quad \text{(Equation 2.4)}$$

where E_{cmto} is the mean concrete modulus of elasticity determined for the time at which the concrete is loaded, and E_{cm28} is the mean concrete modulus of elasticity at a concrete age of 28 days. Within the equations, each model code has different expressions to determine the modulus of elasticity and creep coefficient.

Experimental data have shown that both of the models mentioned underestimate both the shrinkage and creep strains.[29] Alternatively, other studies have shown that the ACI 209 provisions overestimate the creep strains in the short-term while underestimating them in the long term.[30] An alternative method of determining creep and shrinkage strains has been proposed. This method is termed GL2000. When compared to the ACI 209 and CEB-FIP models, the GL2000 model was deemed to most closely fit the experimental data.[31] However, this model has not been incorporated into any of the wood-concrete composite beam rheological models which are described subsequently.

Many rheological models exist for wood. A general method of modeling the time-dependent behavior is to use any number of spring and damper elements connected either in series (Kelvin model, Figure 2.6) or in parallel (Maxwell model, Figure 2.7).

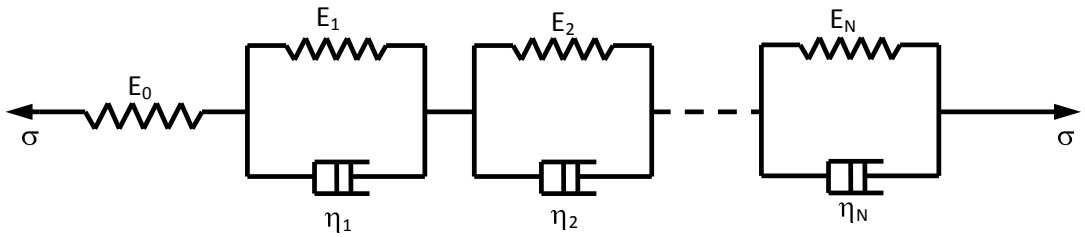

Figure 2.6 Generalized Kelvin Model[17]

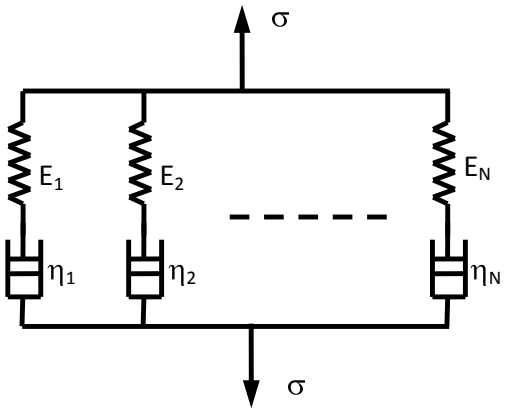

Figure 2.7 Generalized Maxwell Model[17]

In both rheological models, the spring elements account for the elastic behavior while the dashpots account for viscous behavior. The elements of the models have been defined in many different ways. Toratti assumed linear elements and produced an accurate representation for stress levels less than 20% of the strength of the material.[7] Hanhijärvi[25] developed a model which includes non-linear elements and adds an additional shrinkage/swelling component to the generalized Maxwell model. This model required the use of ten parallel Maxwell elements. Zhuoping recognized that the large number of elements in the rheological model results in a large number of rheological parameters that need to be determined.[32] He postulated that the parameters could be variable by making them a function of time.

In order to model the mechanics behavior of wood-concrete composite beams, the effects of all of the related phenomena must be combined and considered simultaneously. There are a number of different methods for achieving this, including linear, nonlinear, finite difference, and finite element models.[6] Here a 1D finite element model developed by Fragiacomo[5] and a 3D finite element model developed by To[17] will be described.

Fragiacomo's model for the long-term behavior of wood-concrete considers the connection to be smeared along the length of the beam.[6,7] Smearing assumes that the connection is a continuous spring between the materials along the length of the beam, and reduces the number of finite elements required to model the beam. The global beam is accurately simulated, but some of the local effects around connections are neglected. The model includes constitutive laws for each of the components of the beam, including the wood, concrete, connections, and reinforcement. The equations are solved in incremental time steps, and the effects are combined to provide the overall behavior of the beam. For the concrete layer, the CEB-FIP Model Code 90 was used for both the shrinkage and creep behavior. For the timber portion of the beam, Fragiacomo's model includes Toratti's rheological model in order to consider the diffusion of moisture into the wood so that the moisture content of the wood can be determined as a function of time. A linear-viscoelastic model with an allowance made for the mechano-sorptive creep was utilized for the

connection system. As the connection tends to experience more creep than the timber, Fragiacomo uses a creep coefficient double that of the timber layer to account for that factor.

Fragiacomo verified his model with several different experimental data sets, including those from the long-term tests done by Fast. When compared to Fast's data, the model predicted the long-term behavior quite well, though it under predicted the elastic deflection of the beam.[33]

In a parallel MPC-supported research study, To[17] developed a 3D finite element model for the time-dependent behavior of wood concrete composite beams. For the wood layer, To used Toratti's linear model. When considering the concrete behavior, the CEB-FIP Model Code 90 was used to predict creep deflection, but the ACI 209-92 code was used to determine the shrinkage. For the shrinkage, the ACI code was used for all times after seven days while experimentally monitored data were used to develop an expression to model the shrinkage during the first seven days. The results from the study were verified by comparing the results of the developed model to the experimental results of his parallel study of the long-term behavior of a wood-concrete composite beam which utilized the notched connection shown in Figure 2.2. The wood layer was composed of a solid layer of dimension lumber. There was very good agreement (see Figure 2.8) between the model and the experimental results. To[17] compared the results of his 3-D model with those of the one-dimensional model developed by Fragiacomo. The three-dimensional model had increased accuracy as compared with the 1-D model; however, the improvement was minimal. Yet, the developed model is an improvement as it does not require that parameters such as the slip modulus and creep coefficient of the connection to be determined experimentally. Also, the 3-D model is far more versatile as it can be applied to different geometries than are possible with the one-dimensional model.

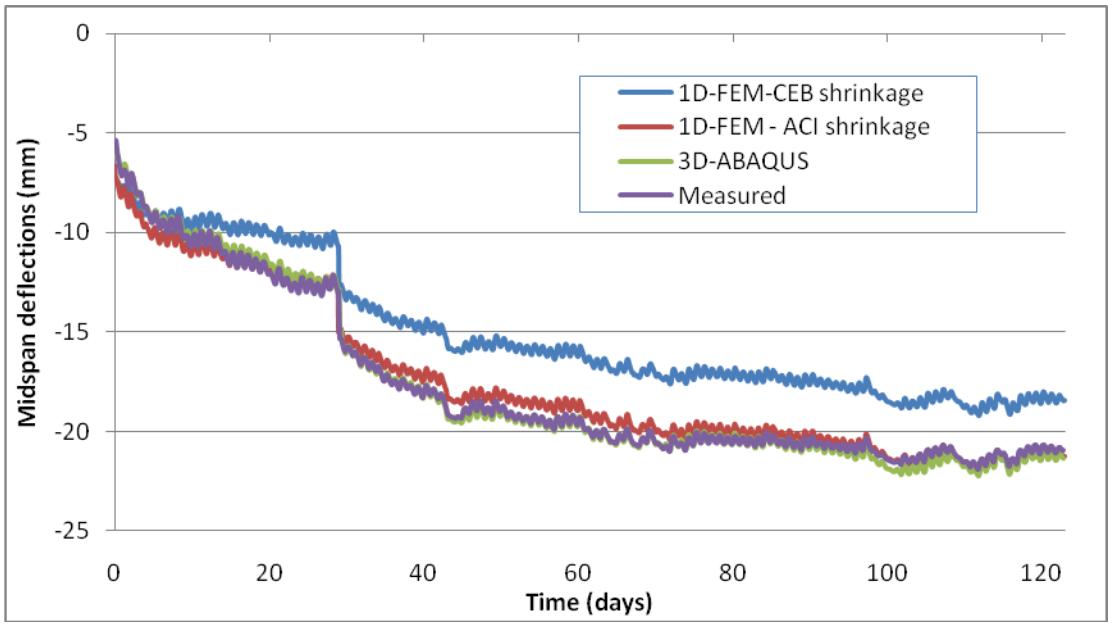

Figure 2.8 Comparison of Experimental Data, 3D Model, and 1D Model[17]

3. TEST SPECIMENS AND CONSTRUCTION

3.1 Specimens

Two laboratory test specimens were utilized in this research study. The first specimen, Specimen M1, served to study the long-term behavior of the specimen under sustained loads in a creep test. The second specimen, Specimen M2, served to study the long-term effects associated with repeated loads. Each specimen was constructed (using essentially the same procedure as LeBorgne[4,5]) with two utility poles as the wood lower portion of the beam and concrete placed on top of the wood. The connections were anchored notches like those used by LeBorgne.

The utility poles used in Specimens M1 and M2 were not identical to those used by LeBorgne. They were donated from a local utility company that had removed the poles from the field. Thus, the size and species of the poles were not within the researchers' control. The clear span for both specimens was set at 295 in. (24 ft. - 7 in.), which is more than 5 ft. shorter than the span used for LeBorgne's specimens.

3.2 Specimen Design

For both specimens, the modulus of elasticity of the wood poles was experimentally measured by applying a midspan point load to the in place pair of poles. Load and midspan deflection were used to determine the modulus of elasticity in accordance with an ordinary mechanics equation.

$$E = \frac{P}{\Delta} * \frac{l^3}{48*I} \qquad \text{(Equation 3.1)}$$

where $\frac{P}{\Delta}$ is the slope of a plot of load versus midspan deflection, l is the clear span length of the beam, and I is the moment of inertia of the wood poles. This calculation neglects any contribution from shear deformation. Based on the calculation for the modulus of elasticity, the likely species of the utility poles for each specimen was assessed. Table 6B in the NDS wood code[23] presents species of wood poles with their modulus of elasticity values. The species of the poles were deduced based on Table 6B and each one chosen is known to be one of the two species predominantly used to manufacture utility poles. Table 3.1 shown below presents the measured modulus of elasticity, assumed species, and measured dimensions of the wood poles used for the two specimens.

Table 3.2 Wood Pole Details

	Specimen M1	Specimen M2
Modulus of Elasticity	1905000 psi	1238000 psi
Assumed Species	Douglas Fir	Ponderosa Pine
Average Midspan Diameter	10.3 in	11.345 in
Clear Span	295 in	295 in

Based on the values in Table 3.1, the design procedure developed by LeBorgne[4] was used to complete the configuration of the specimens. An example of the design program spreadsheet and computations, taken from Specimen M2, is provided in Appendix A. Figures 3.1 and 3.2 show the layout of the specimens with the dimensions labeled. Table 3.2 provides the important dimensions as well as the designed capacity of each specimen.

Table 3.3 Selected Design Parameters for each Specimen

	Specimen M1	Specimen M2
Span, L	295 in	295 in
Wood Diameter, dw	10.3 in	11.345 in
Notch 1, Ln1	32 in	28 in
Notch 2, Ln2	60 in	61 in
Notch 3, Ln3	128 in	123 in
Notch Length, ln	9 in	9 in
Notch Height, hn	2.75 in	3 in
Notch Angle, Θn	10 deg	10 deg
Reinforcement Depth, dr	3.5 in	3.25 in
Concrete Height, hc	7 in	6.5 in
Concrete Width, wc	21.5 in	23.5 in
Concrete Strength, f´c	5000 psi	5000 psi
Concrete Modulus of Elasticity, Ec	4030000 psi	4030000 psi
Maximum Moment, Mmax	2045 kip-in	1522 kip-in
Maximum Point Load, Pu	24.45 kip	17.12 kip
Design Service Load, Pa	15.28 kip	10.70 kip

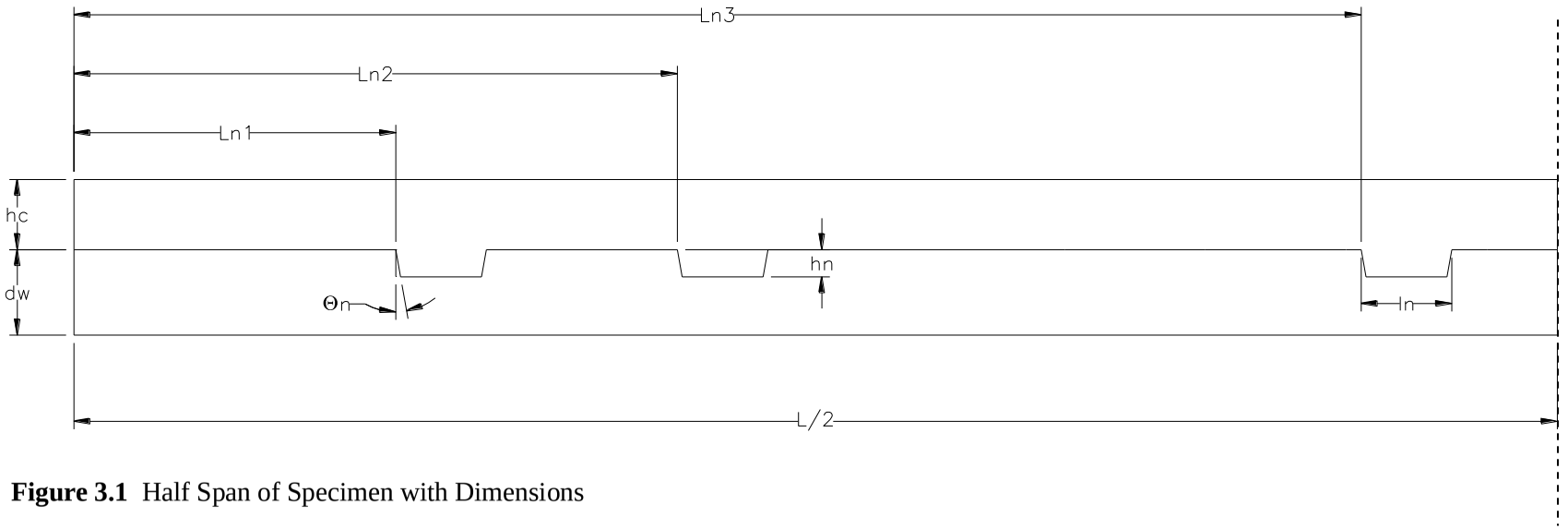

Figure 3.1 Half Span of Specimen with Dimensions

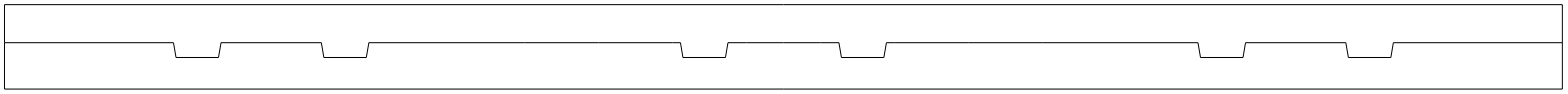

Figure 3.2 Full Specimen

LeBorgne's design program is based on an assumed concrete strength of 5000 psi. The modulus of elasticity is determined based on the ACI equation using the strength of the concrete, Equation 3.2, where f_c' is the concrete compressive strength in psi.

$$E_c = 57000 * \sqrt{f_c'} \qquad \text{(Equation 3.2)}$$

The properties of the delivered concrete will vary somewhat based on how closely the concrete batches actually match the specified mix design. Standard 6 in. diameter cylinders were cast (in accordance with ASTM C192-98[34]) at the time that the concrete was placed and tested in compression in accordance with ASTM C39-96[35] at an age of 28 days. Using the data from the compression test, the actual compressive strength and the modulus of elasticity were determined for the delivered concrete batches. Table 3.3 below provides the data from the compression tests of the concrete cylinders. For accuracy in the analysis of the designs, the values for the strength and modulus of elasticity based on cylinder tests were input into LeBorgne's spreadsheet rather than the above specified design values. Table 3.4 lists the resulting capacities determined for each specimen revised for the new concrete parameters. Notice in Table 3.3 that there is a significant difference in the tested strength of the concrete in each specimen, though they had the same specified design strength of 5 ksi. This is likely, in part, due to too much water being added to the mix in Specimen M1, which is a result of the concrete being delivered commercially rather than being mixed on site.

Table 3.4 Concrete Cylinder Tested Properties

Specimen M1			Specimen M2		
Cylinder	Strength (ksi)	MOE (ksi)	Cylinder	Strength (ksi)	MOE (ksi)
1	4.75	3348.8	1	6.97	4021.1
2	4.93	3295.8	2	6.96	3743.5
3	4.91	3199.2	3	6.75	3713.7
Average	4.86	3281.3	Average	6.89	3826.1

Table 3.5 Revised Design Results

	Specimen M1	Specimen M2
Maximum Moment, Mmax	2005 kip-in	1515 kip-in
Maximum Point Load, Pu	23.90 kip	17.03 kip
Design Service Load, Pa	14.94 kip	10.64 kip

In his design method, LeBorgne employs a moment reduction factor applied to the moment capacity to account for the partially composite section. In configuring the specimens herein, the moment reduction factor was neglected, as it had no significant effect on the member moment capacity.

4. TEST PROCEDURES

4.1 Creep Test

After the concrete was placed, the beam was ready for the monitoring and testing procedures. The finished beam for the creep test is shown in Figure 4.1. At a time of 28 days after casting, the anchor dowels were retightened to a torque of 25 ft.-lb. This was done to assist in closing any gap that may have formed between the concrete and wood as the concrete cures and to resist any upward forces that may result from the sloped sides of the notches.

Figure 4.9 Completed Wood-Concrete Composite Beam (Specimen M1)

The vertical position of both specimens was monitored as soon as the concrete was placed. For Specimen M1, string potentiometers were used to measure deflection and were attached to each pole at midspan and close to each end. A data logger recorded these measurements in ten minute intervals. Specimen M2 was instrumented the same but without a data logger. Deflection measurements were taken manually with a computer in varying increments of approximately 24 hours.

Two aspects were considered in the creep test, Specimen M1: creep during the 28-day concrete curing period and long-term creep under additional applied live load. During the 28-day period, the temperature, humidity, and deflection of the beam were recorded. These data were obtained to develop an empirical formula that could be used to approximately predict creep during that period. LeBorgne had developed an empirical equation for the specimens in his study; however, the data obtained in this study was added to his data set to revise and improve the accuracy of his equation

For the long-term creep test, Specimen M1 was loaded with a constant live load after the concrete had cured for 28 days. The specimen was allowed to creep under this load for 256 days while the deflection, temperature, and humidity were monitored. To remain consistent with Fast, the specimen was loaded to approximately 11% of the ultimate design capacity of the beam. The beam was to be loaded with concrete cylinders each with a 14 in. diameter, and the weight of the cylinders varied between 443 lb. and 448 lb. with an average weight of 445 lb. The cylinders were placed on top of the specimen lying on their

sides across the specimen and were assumed to be a uniformly distributed load of 445 lb./14 in. or .0318 kip/in. The internal moment created was determined from Equations 2.1 and 2.2.

$$R_1 = \frac{w*b}{2} \quad \text{(Equation 2.1)}$$

$$M_{max} = R_1 * \left(a + \frac{R_1}{2*w}\right) \quad \text{(Equation 2.2)}$$

Equation 2.1 determines the reaction, R_1, at one of the end supports where ***w*** is the magnitude of the uniformly distributed load and ***b*** is the length of the distributed load on the beam. Equation 2.2 determines the maximum moment in the beam where ***a*** is the length of the beam on either end of the distributed load that is not loaded. From these equations, it was determined that eight cylinders would be necessary. Figure 4.2 shows Specimen M1 with the concrete cylinders applied as the live load.

Figure 4.10 Specimen M1 Loaded with Live Load

The specimen was instrumented with dial gages (see Figure 4.3), accurate to ±0.0001 in., on the ends of the specimen to monitor slip between the wood and the concrete. Data from the long-term creep test can be used, in part, to determine possible camber requirements based on the long-term deflection of the specimen.

Figure 4.11 Slip Instrumentation on Specimen M1

4.2 Repeated Load Test

After the 28-day curing period, Specimen M2 was subjected to a repeated loading test. A hydraulic actuator was used to apply a line load across the width of the beam at midspan (see Figure 4.4). The actuator was operated using a sine wave to load the beam between just above zero load and the design service load, 10.64 kips, with some small variations (approximately 10-11 kips on the high end and .5-1 kip on the low end). Figure 4.5 shows the representative repeated loads used for testing Specimen M2. The cyclic loading was performed with a frequency of 0.25 cycles per second.

Figure 4.12 Test Set Up for the Specimen M2 Repeated Loading Test

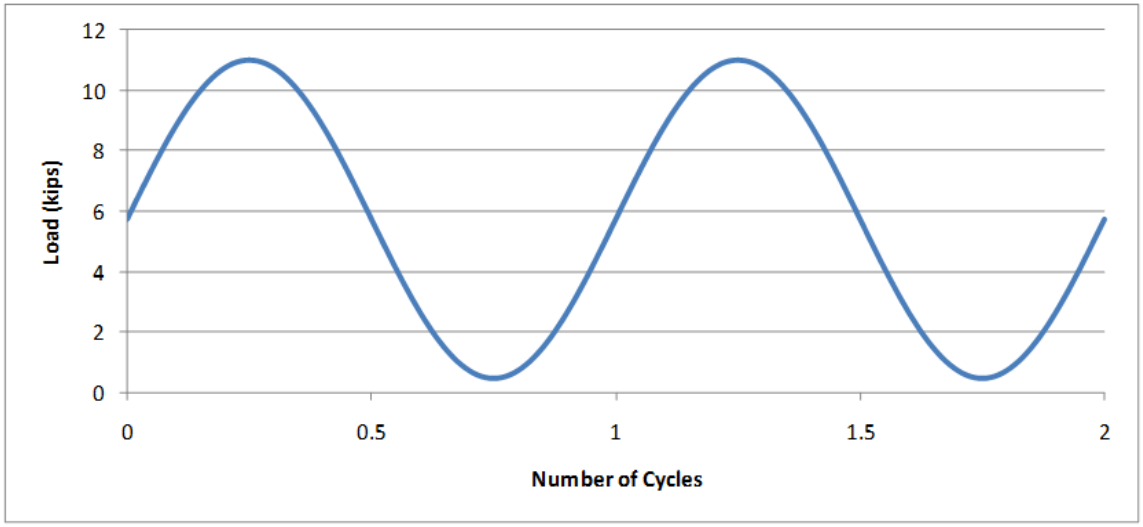

Figure 4.13 Sine Wave Used for Loading Specimen M2

Changes in the stiffness of the specimen were monitored as well as any permanent deflections that were incurred. For the first 15,000 cycles, the specimen was loaded in sets of 2,500 cycles, and the stiffness and deflection of the beam were checked after each set. After 15,000 cycles, the sets were increased to 5,000 cycles. The cycles were stopped after 35,000 cycles had been completed as very small changes in the beam stiffness were occurring at that point in time.

4.3 Composite Efficiency

At various times, the cyclic loading of Specimen M2 was stopped. A known load was applied and the deflection was measured. The theoretical fully-composite and non-composite deflections were computed. The EFF was then calculated using Equation 2.1. For Specimen M1, the efficiency was found at the time of the live load application. Results are presented and discussed subsequently.

5. RESULTS AND ANALYSIS

5.1 28-Day Creep Test

During the 28-day curing period of the concrete, the deflections of Specimens M1 and M2 were monitored under the applied dead load of the concrete layer. The temperature and relative humidity of the testing environment were also recorded. Figure 5.1a and 5.1b depict the data for Specimen M1. Figure 5.1a illustrates the time-dependent deflection of Specimen M1 together with the temperature. Figure 5.1b provides the time-dependent deflection of Specimen M1 together with the relative humidity data. Figures 5.2a and 5.2b are the counterpart plots for Specimen M2. The deflection that is plotted is only the time-dependent deflection. The initial short-term deflection has been subtracted from the data.

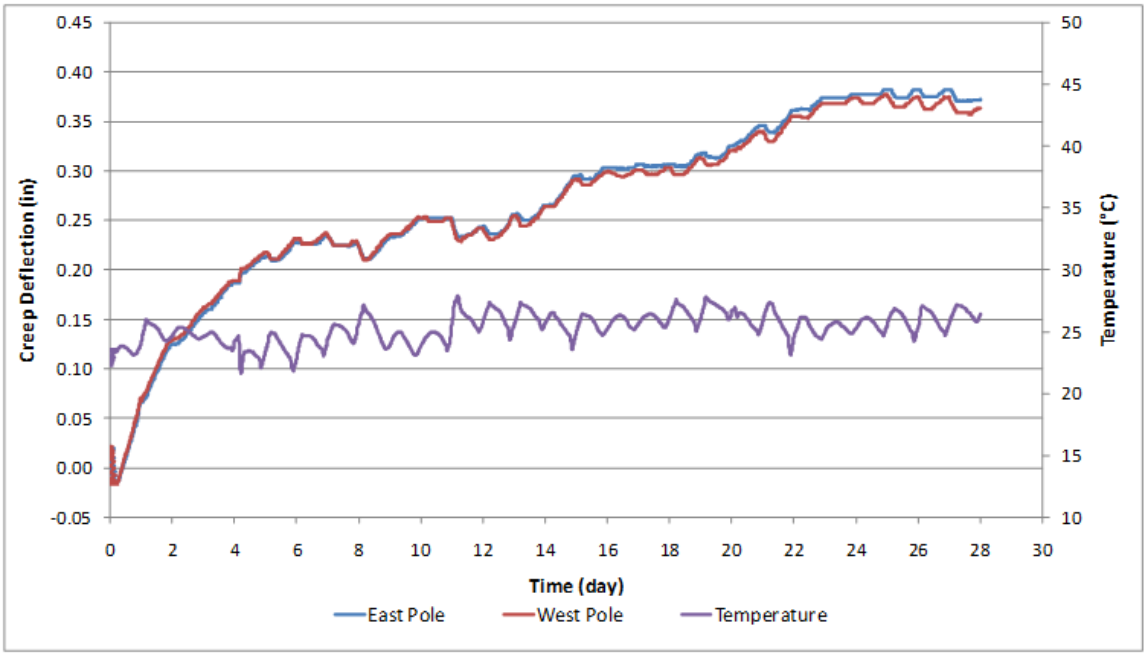

Figure 5.1a: Specimen M1 Creep Deflection with Temperature Data

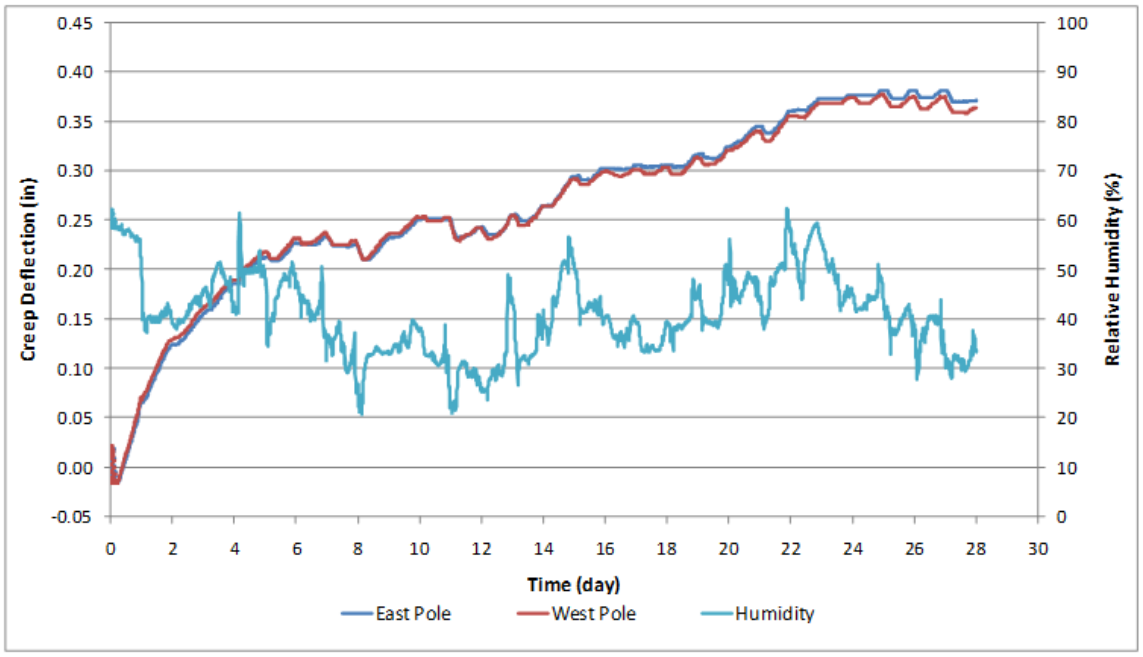

Figure 5.1b Specimen M1 Creep Deflection with Relative Humidity Data

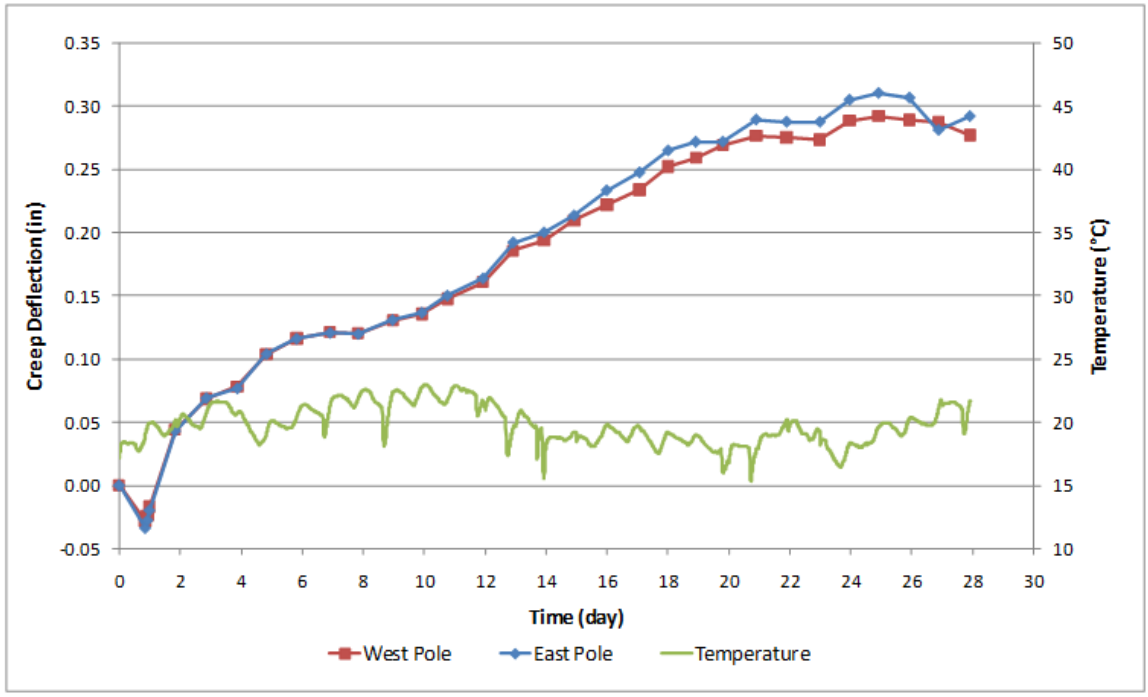

Figure 5.2a Specimen M2 Creep Deflection with Temperature Data

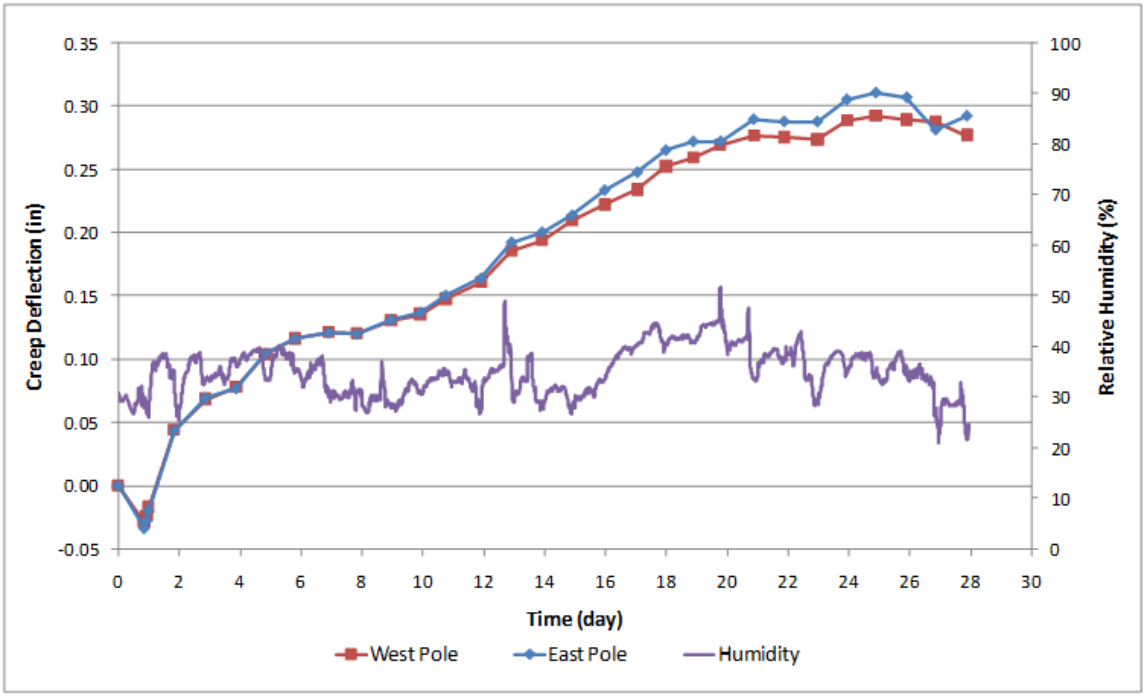

Figure 5.2b Specimen M2 Creep Deflection with Relative Humidity Data

The preceding figures display a typical creep behavior for the time-dependent deflection of each specimen. The deflection steadily increased and then generally increased at a slower rate later in the period. Data for Specimen M1 are more complete than the data for Specimen M2 as a data logger recorded the temperature, humidity, and deflection every ten minutes. Due to limitations in the instrumentation available for Specimen M2, the deflection measurements were logged at a much slower rate, which was typically once per day.

Figures 5.1a and 5.1b indicate that there is an oscillation in deflection that occurs as the temperature and humidity oscillate. Only the combined effect can be observed. It cannot be determined what amount of the effect results from the changes in temperature vs. humidity alone. Thus, the observed oscillations must be considered as a function of both the temperature and relative humidity.

To better understand the oscillation in the temperature and humidity, Figure 5.3 provides a magnification of the temperature and humidity record for Specimen M1. The temperature is shown in blue and is plotted on the left axis. The relative humidity is shown in red and is plotted on the right axis. The temperature varies between approximately 21.5°C and 28°C while the relative humidity varies between approximately 20% and 65%. The figure shows that there is generally an inverse relationship between the relative humidity and temperature. In times of increased temperature, there is typically decreased relative humidity, and vice versa. Although this behavior predominates, it is not completely consistent throughout the monitored time period.

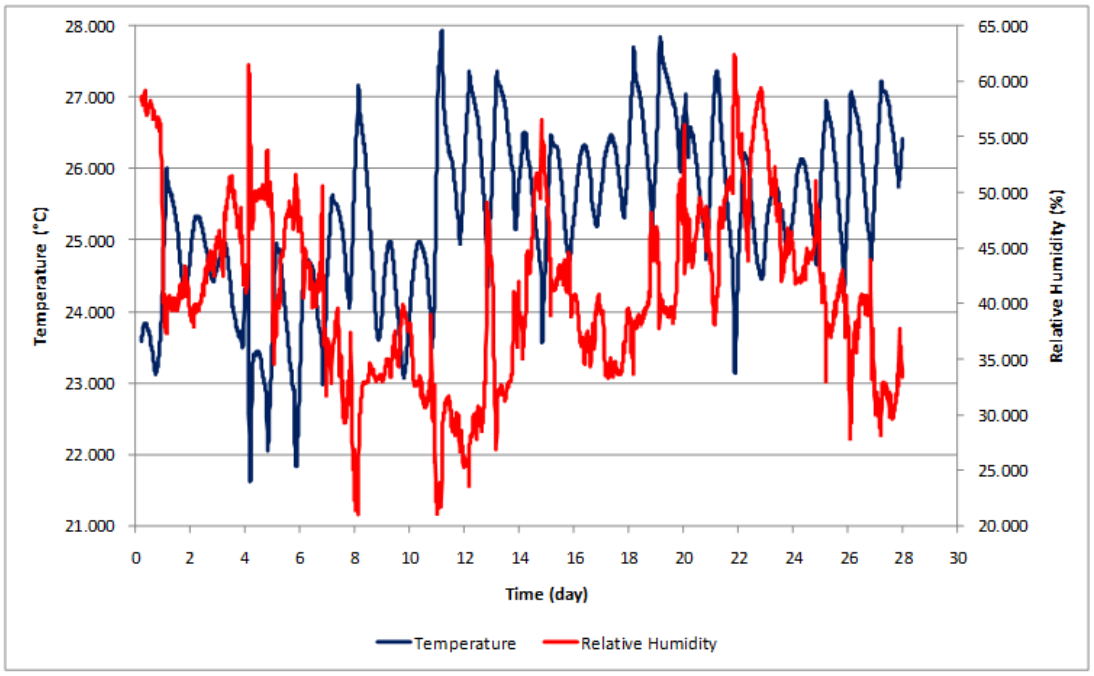

Figure 5.3 Temperature and Relative Humidity Variation for Specimen M1

Referring again to Figures 5.1a and 5.1b, the observed trend is that the oscillation in deflection is inversely related to the temperature and directly related to the relative humidity. Also, in periods of large increases in humidity and/or decreases in temperature, there is a corresponding larger relative increase in the deflection of the specimen. While Specimen M2 does not exhibit the effect of the oscillations, it is evident that large decreases in the temperature and/or increases in the humidity result in larger increases in the deflection of the specimen.

For both Specimen M1 and Specimen M2, shortly after the initial short-term deflection, there is a negative creep deflection (an upward deflection). This phenomenon was not observed for LeBorgne's specimens (using utility poles for the wood layer); however, it was observed for Fast's specimens (using dimensioned lumber). In Fast's specimens, as well as in Specimens M1 and M2, this is believed to have resulted from the increased temperature of the concrete layer as a result of the chemical reactions associated with the concrete curing process. As the temperature of the concrete layer increases, thermal strains result in the lengthening of the slab. Due to the interconnection of the layers by the notched connection, the composite beam deflects upward as a result of the horizontal shear stresses created at the top of the wood layer due to the thermal strains.[33]

Figure 5.4 shows the overall deflection data (average of the midspan deflections of the two poles) for the 28-day concrete curing period for both the specimens in this study, Specimens M1 and M2, as well as the specimens from LeBorgne's study, Specimens L1 and L2. The figure includes the initial short-term deflection due to the self-weight of the concrete layer on the beam. It is evident that deflection due to time-dependent effects constitutes a significant portion of the overall deflection of the wood-concrete composite beam specimens. For the four specimens in Figure 5.4, the magnitude of the time-dependent deflection at the end of the 28-day period was between 28% and 65% of the initial short-term deflection due to the self-weight of the concrete layer on the utility poles. Clearly, there is a large difference in the magnitude of the time-dependent deflection experienced by each specimen. The NDS and ACI design codes include empirical equations for predicting time-dependent deflection of wood and concrete alone (as individual materials), respectively. These approaches are examined below.

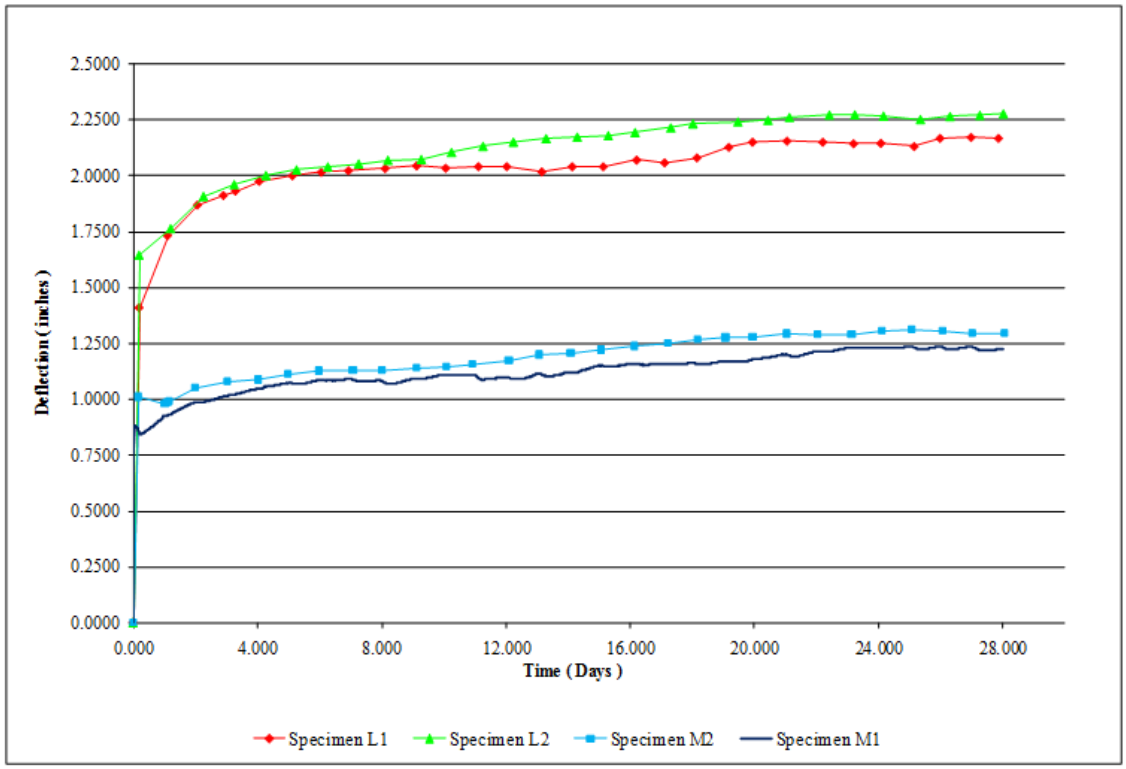

Figure 5.4 28-Day Deflection of all Specimens

The NDS code only provides an equation (Equation 5.1) for determining the total deflection of a wood beam subjected to a long-term applied load.

$$\Delta_T = (K_{cr} * \Delta_{LT}) + \Delta_{ST} \qquad \text{(Equation 5.1)}$$

In Equation 5.1, Δ_T is the total deflection of the beam, Δ_{ST} is the immediate deflection due to the short-term component of the design load, Δ_{LT} is the immediate deflection due to the long-term component of the design load, and K_{cr} is the time-dependent deformation factor. The time-dependent deformation factor for the utility poles is 1.5. This means that Equation 5.1 predicts the total deflection due to sustained loads would be 1.5 times the elastic deflection due to those loads. The NDS code only provides for the ultimate creep value while not specifically dealing with the variation of the creep deflection over time.

The ACI 318 code includes an equation to account for time-dependent deflections for reinforced concrete beams. Equations 5.2 and 5.3 constitute the ACI method.

$$\Delta_{creep} = \Delta_{elastic} * \lambda_\Delta \qquad \text{(Equation 5.2)}$$

$$\lambda_\Delta = \frac{\xi(t)}{1+50*\rho'} \qquad \text{(Equation 5.3)}$$

In these equations, Δ_{creep} is the deflection that results from creep, $\Delta_{elastic}$ is the elastic deflection due to the application of the sustained load, λ_Δ is the multiplier for additional deflection due to long-term

effects, $\xi(t)$ is the time-dependent factor for sustained loads, and ρ' is the compression reinforcement ratio. For times less than 28-days, the value of $\xi(t)$ is not defined by the ACI 318 code. Therefore, the ACI prediction method assumes that the load is applied after the 28-day concrete curing period and does not consider the creep deflection under the self-weight of the concrete as it cures.

The NDS and ACI deflection prediction methods provide long-term creep deflection predictions for wood and concrete, respectively. They do not provide formulations that allow for the deflection of the materials to be predicted at various times within the 28-day concrete curing period. In order to account for this a different method of prediction must be used.

LeBorgne[4,5] developed an empirical equation for predicting the deflection of a wood-concrete composite beam during the 28-day concrete curing period. The equation is based on a logarithmic approximation to the creep data from one of his specimens, namely, his Specimen L2. A logarithmic curve was empirically fit to the deflection due to creep data (total deflection minus initial elastic deflection). This expression is provided in Equation 5.4.

$$\delta_{emp\_creep} = 0.1544 * \ln(t) + 0.12486 \qquad \text{(Equation 5.4)}$$

Since this equation is specific to Specimen L2, it was necessary to generalize the expression for various specimen configurations. To do so, similar to LeBorgne, it was theorized that the effect of creep could be expressed as a uniform load that varied in magnitude as a function of time. To do this, Equation 5.4 is set equal to the ordinary mechanics equation for the deflection of a simply supported beam with a uniform load, i.e.,

$$\delta_{emp\_creep} = \frac{5*\omega_{creep}*L^4}{384*E_w*I} \qquad \text{(Equation 5.5)}$$

where δ_{emp_creep} is the empirical expression for the deflection due to creep as a function of time, L is the span of Specimen L2, E_w is the modulus of elasticity of the wood poles for Specimen L2, $\bar{I}$ is the moment of inertia of the transformed section of Specimen L2, and ω_{creep} is the equivalent uniform creep load as a function of time. Setting Equations 5.4 and 5.5 equal to each other, the effective uniform creep load results, namely,

$$\omega_{creep} = 16.80141 * \ln(t) + 13.58695 \qquad \text{(Equation 5.6)}$$

Thus, for a generic cross-section, the deflection due to creep can be found using the equation for deflection provided in Equation 5.7. The total deflection for any time after the initial short-term deflection is given by the sum of the short-term deflection due to the self-weight of the concrete and the deflection due to creep (Equation 5.8). This is the equation proposed by LeBorgne for the prediction of the deflection due to creep in the first 28 days.

$$\delta_{creep} = \frac{5*[16.8014*\ln(t)+13.5869]*L^4}{384*E_w*\bar{I}} \qquad \text{(Equation 5.7)}$$

$$\delta_{total} = \frac{5*\omega_c*L^4}{384*E_w*I_w} + \frac{5*[16.8014*\ln(t)+13.5869]*L^4}{384*E_w*\bar{I}} \qquad \text{(Equation 5.8)}$$

In Equation 5.8, ω_c is the uniformly distributed dead load of the concrete, L is the clear span of the specimen, E_w is the modulus of elasticity of the wood poles, I_w is the moment of inertia of the wood poles, and $\bar{I}$ is the moment of inertia of the transformed section of the composite cross section. The transformed section is determined based on the modulus of elasticity of the concrete at an age of 28 days. It should be noted that Equation 5.8 is empirically based on 28-day deflection data. LeBorgne only intended that it be valid over the 28-day curing period of the concrete. Table 5.1 provides the parameters used for the prediction in Equation 5.8. The resulting predictions for each of LeBorgne's specimens (L1 and L2) are illustrated in Figure 5.5 and compared to his actual measured data. The predicted responses closely approximate the trends of the measured data except for the first 7 days of Specimen L1 where the deflection is under predicted. At the end of the 28-day period, the difference between the measured and predicted values is less than 3% for each specimen. Table 5.2 and 5.3 provide a comparison between the measured and predicted deflections at certain times during the 28-day concrete curing period. In the comparison, the percentage difference is calculated as shown in Equation 5.9

Table 5.1 Specimen Dimension and Mechanical Properties

		Specimen L1	Specimen L2	Specimen M1	Specimen M2
ω_c	(lb/in)	15.0	15.8	15.4	16.1
L	(in)	354.24	354.24	295.00	295.00
E_w	(psi)	1106500	1966000	1905000	1238000
I_w	(in^4)	1952	982	1105	1626
$\bar{I}$	(in^4)	16084	11349	9753	14553

$$\% \, Difference = \frac{\delta_{measured} - \delta_{predicted}}{\delta_{measured}} * 100 \qquad \text{(Equation 5.9)}$$

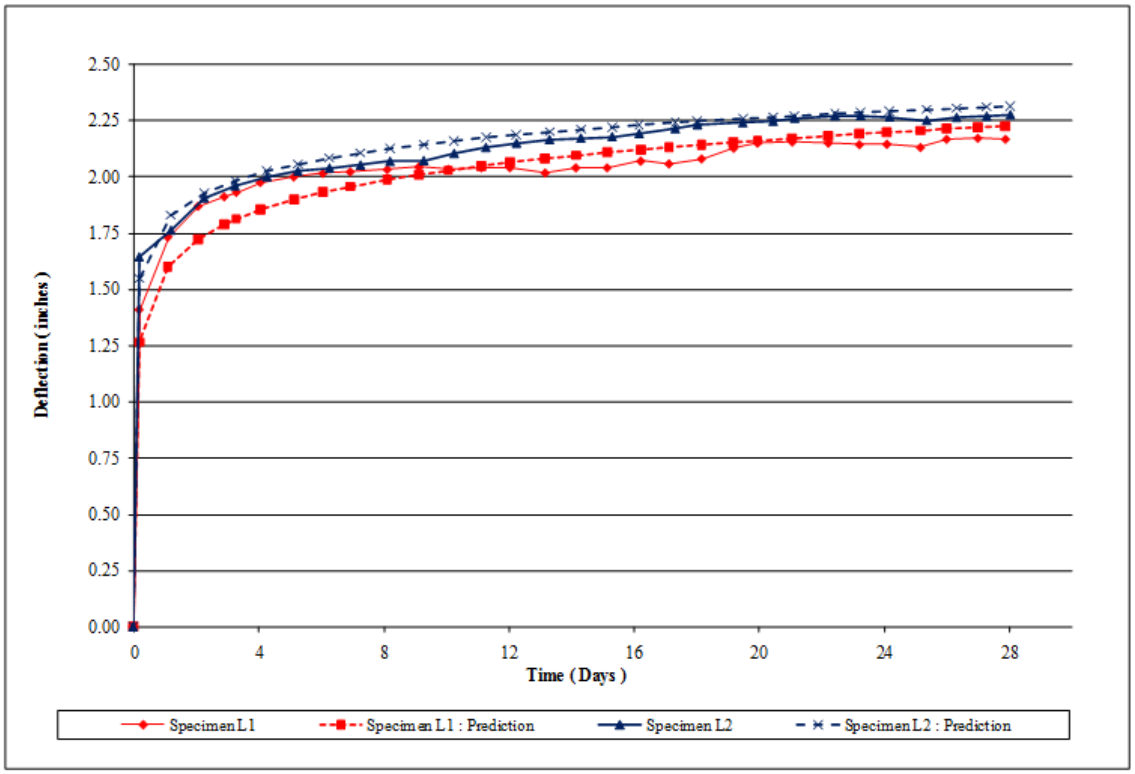

Figure 5.5 Creep Response of LeBorgne Specimens - Measured vs. Predicted (Equation 5.8)

Table 5.2 Specimen L1 Comparisons

Time	Deflections (in)			% Difference
	Measured	Predicted (Eq. 5.8)	Difference	
Elastic	1.410	1.265	0.145	10.28%
7 days	2.022	1.955	0.067	3.31%
14 days	2.040	2.093	-0.053	-2.60%
21 days	2.155	2.170	-0.015	-0.70%
28 days	2.167	2.224	-0.057	-2.63%

Table 2.3 Specimen L2 Comparisons

Time	Deflections (in)			% Difference
	Measured	Predicted (Eq. 5.8)	Difference	
Elastic	1.644	1.546	0.098	5.96%
7 days	2.052	2.104	-0.052	-2.53%
14 days	2.172	2.209	-0.037	-1.70%
21 days	2.260	2.269	-0.009	-0.40%
28 days	2.276	2.313	-0.037	-1.63%

When Equation 5.8 is applied for Specimens M1 and M2, while providing the correct trend over time, it significantly underestimates the deflection. Figure 5.6 shows the differences between the predictions and the actual data. Tables 5.4 and 5.5 provide numerical comparisons between the measured and predicted

deflections at selected times during the 28-day concrete curing period. At the end of the 28-day period, there are 11% and 10% errors between the actual data and the prediction for Specimen M1 and Specimen M2, respectively.

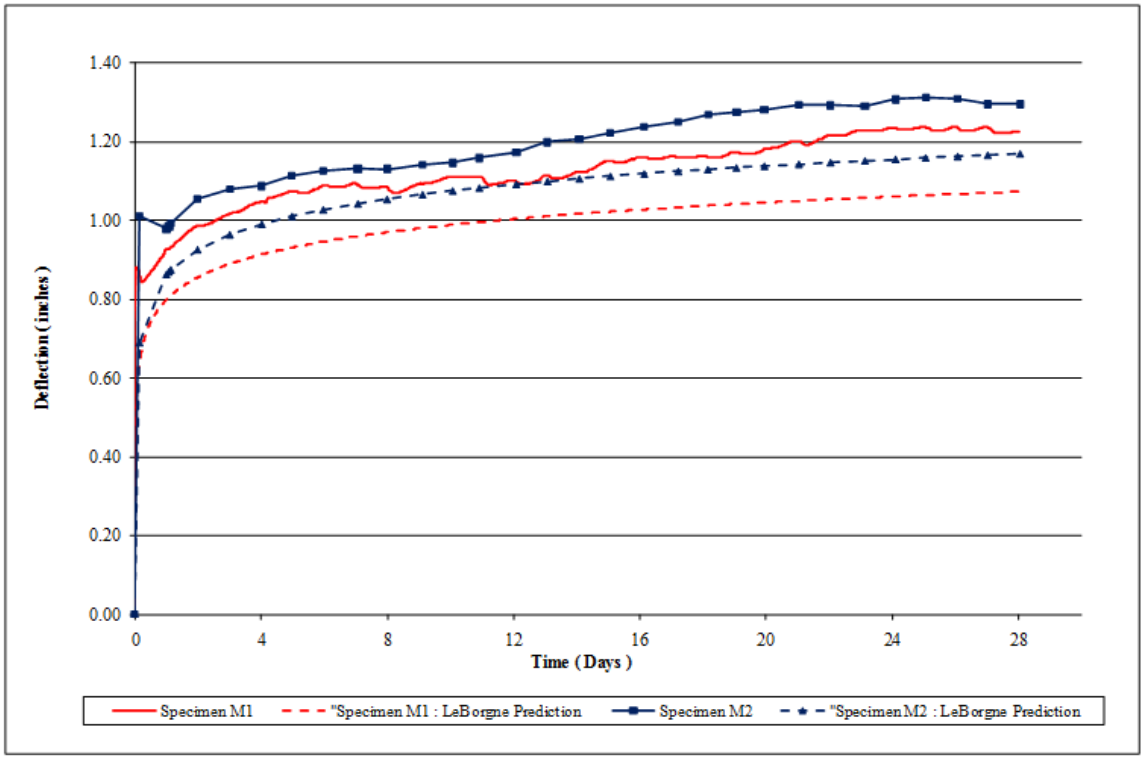

Figure 5.6 LeBorgne's Prediction Applied to Specimen M1 and Specimen M2 (Equation 5.8)

Table 5.4 Specimen M1 Comparisons

Time	Deflections (in)			% Difference
	Measured	Predicted (Eq. 5.8)	Difference	
Elastic	0.746	0.721	0.025	3.35%
7 days	1.094	0.967	0.127	11.61%
14 days	1.123	1.029	0.094	8.37%
21 days	1.202	1.065	0.137	11.40%
28 days	1.227	1.091	0.136	11.08%

Table 5.5 Specimen M2 Comparisons

Time	Deflections (in)			% Difference
	Measured	Predicted (Eq. 5.8)	Difference	
Elastic	1.009	0.789	0.220	21.80%
7 days	1.130	1.042	0.088	7.79%
14 days	1.206	1.106	0.100	8.29%
21 days	1.292	1.143	0.149	11.53%
28 days	1.294	1.169	0.125	9.66%

Clearly, directly applying Equation 5.8 to Specimens M1 and M2 is inadequate. The error between the predicted and measured values of deflection is attributed to the differences in the span of the specimens compared with LeBorgne's specimens. Equation 5.8 is a function of the clear span, modulus of elasticity, and moment of inertia of the composite section. It is likely that a portion of the creep deflection approximated by Equation 5.4 is not a function of the clear span. One example of this is the effect of the heating of the concrete layer as it cures. The temperature of the concrete layer has an impact on the deflection of the specimen; however, the temperature increase is not a function of L^4 as Equation 5.8 would suggest. Thus, a modification to Equation 5.8 is recommended to account for this.

The modification begins in the same manner as LeBorgne's method using the empirical equation for the deflection due to creep (Equation 5.4). However, the equation is separated into two parts that are treated individually. The first part is the logarithmic term of the approximation. This term of the approximation accounts for the creep and shrinkage effects of the concrete layer as well as the creep and mechanosorptive creep of the wood layer and connection. Thus, it is treated in the same manner as done by LeBorgne.[4,5] The constant term of the approximation equation is assumed to correspond to the deflection that occurs early on in the test period from the increase in temperature of the concrete layer as it cures. The heating of the concrete layer has been observed in the construction of steel-concrete composite bridges,[36] and it has been noted that this has an impact on the deflection of wood-concrete composite bridges.[33] This phenomenon is not a function of length. However, herein this deflection is assumed to be a function of the modulus of elasticity of the wood layer and the moment of inertia of the transformed composite section. Thus, Equation 5.6 can be recast with an adjustment made to the constant term to eliminate its dependence on the clear span of the specimen. See Equation 5.10. The adjustment in Equation 5.10 is such that the second term reflects the ratio of LeBorgne's span to L, the span of the specimen in question. When this is done, the spans will cancel in formulating the full equation of the total deflection of the specimen. See Equation 5.11a. This equation can then be simplified into its final form, Equation 5.11b, whereby the span is not present in the second term.

$$\omega_{creep} = 16.80141 * \ln(t) + 13.58695 * \left(\frac{354.24^4}{L^4}\right) \quad \text{(Equation 5.10)}$$

$$\delta_{total} = \frac{5*\omega_c*L^4}{384*E_w*I_w} + \frac{5*[16.8014*\ln(t)+13.5869*\left(\frac{354.24^4}{L^4}\right)]*L^4}{384*E_w*I} \quad \text{(Equation 5.11a)}$$

$$\delta_{total} = \frac{5*\omega_c*L^4}{384*E_w*I_w} + \frac{5*[(16.8014*\ln(t)*L^4)+(213.95*10^9)]}{384*E_w*I} \quad \text{(Equation 5.11b)}$$

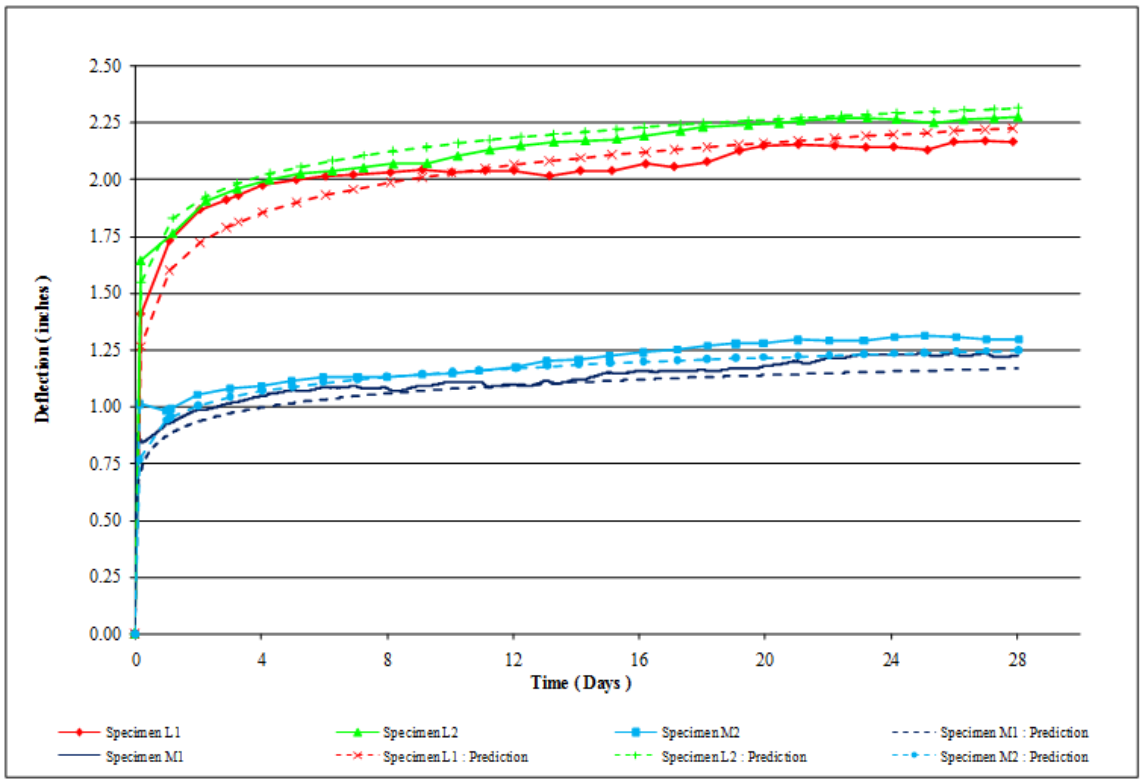

Figure 5.7 Data and Prediction for All Specimens (Equation 5.11)

Figure 5.7 provides a comparison between the measured data and the predictions for deflection over the 28-day concrete curing period for all specimens using Equation 5.11b. As the adjustment term is unity in his cases, the results for the LeBorgne specimens are the same as the prediction using Equation 5.8. However, the predictions for Specimens M1 and M2 change and are noticeably improved. Tables 5.6 and 5.7 provide a numerical comparison between the predicted and the measured deflections at selected times during the 28-day concrete curing period.

Table 5.6 Specimen M1 Comparisons (Equation 5.11)

Time	Deflections (in)			% Difference
	Measured	Predicted (Eq. 5.11)	Difference	
Elastic	0.746	0.721	0.025	3.35%
7 days	1.094	1.047	0.047	4.30%
14 days	1.123	1.109	0.014	1.25%
21 days	1.202	1.145	0.057	4.74%
28 days	1.227	1.170	0.057	4.65%

Table 5.7 Specimen M2 Comparisons (Equation 5.11)

Time	Deflections (in)			% Difference
	Measured	Predicted (Eq. 5.11)	Difference	
Elastic	1.009	0.789	0.220	21.80%
7 days	1.130	1.121	0.009	0.80%
14 days	1.206	1.185	0.021	1.74%
21 days	1.292	1.221	0.071	5.50%
28 days	1.294	1.248	0.046	3.55%

The "measured elastic" deflection listed in each table corresponds to the deflection some time after the concrete was placed. It is not from the exact instant of the initial elastic deflection, as the deflection could not be recorded at the exact instant that the concrete was placed. Consequently, the measured elastic deflection includes some amount of creep deflection, and the predicted value of elastic deflection may under-predict the measured value. This is evident Tables 5.6 and 5.7 as the largest error observed was in the elastic deflection of specimen M2. This may be due, in part, to the presence of some creep deflection in the "elastic deflection" comparison.

Note that the logarithmic term of Equation 5.11b is negative for all time less than one day. This prediction method should only be used to predict the elastic deflection and the total deflection for times greater than one day. Therefore, Equations 5.12 and 5.13 should be used depending on the time in question.

$$\delta_{total} = \frac{5*\omega_c*L^4}{384*E_w*I_w} \quad for \;\; 0 \leq t < 1 \qquad \text{(Equation 5.12)}$$

$$\delta_{total} = \frac{5*\omega_c*L^4}{384*E_w*I_w} + \frac{5*[16.8014*\ln(t)+13.5869*\left(\frac{354.24^4}{L^4}\right)]*L^4}{384*E_w*I} \quad for \;\; 1 \leq t \leq 28 \qquad \text{(Equation 5.13)}$$

Any empirical equation used to predict creep over time will have a certain amount of error inherent in it as a result of the complexity of the rheological phenomena occurring in the specimen. Many variables contribute to changes in the creep deflection other than simply the time duration. The largest contributors are temperature and specimen moisture content. From the data gathered in this study, it was observed that the deflection reflects both the temperature and the humidity exposure conditions of the specific surrounding environment. Therefore, if the specimen was constructed exposed to a different environment and there was a large difference in temperature and/or humidity history, the equations may not provide an accurate prediction. Even with the same environment, there are variations in the deflection as a result of daily changes in temperature and humidity. Therefore, this method should be used with caution as it is likely that there will be inherent error in the prediction that may be considerably non-conservative. To achieve higher accuracy in predictions of time-dependent deflections in wood-concrete composite beams, more rigorous analysis methods must be used. As stated earlier, 1D and 3D finite element models have been incorporated to provide accurate predictions of time-dependent deflections in wood concrete composite beams. Additionally, Fragiacomo[37] has proposed a simplified method of analysis. Consequently, the method of deflection prediction proposed above is only directly useful in an environment very similar to that of the environment that existed during this particular load testing.

5.2 Composite Efficiency

On the 29th day after the placement of the concrete, each specimen was subjected to an applied loading. Specimen M1 was loaded with permanent live load for the creep test while Specimen M2 was ramp loaded to determine the initial stiffness of the specimen for the repeated load tests. Using the known loads and the measured deflections, the composite efficiencies were calculated using Equation 2.1.

Specimen M1 was loaded with eight concrete cylinders as depicted in Figure 5.8. Each cylinder was 14 in. in diameter. The approximate weight of each cylinder was 445 lb. Table 5.8 lists the actual weights. They were placed perpendicular to the longitudinal axis of the specimen and positioned symmetrically about midspan of the specimen. The measured deflection of the beam under this applied load was 0.0997 in.

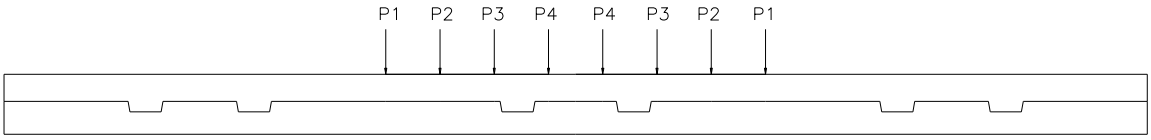

Figure 5.8 Layout of Load on Specimen M1

Table 5.8 Magnitude of Loads on Specimen M1

	Left Load (lbs)	Right Load (lbs)	Average (lbs)
P1	448	444	**446.0**
P2	445	443	**444.0**
P3	444	447	**445.5**
P4	445	444	**444.5**

The theoretical deflection values (for both fully-composite and non-composite states) were calculated using Equation 5.14, which is the ordinary mechanics equation for a series of point loads placed symmetrically about midspan of a simply supported beam. The weights of the concrete cylinders used to load the specimen vary by a few pounds. To account for this, the average weight of the two cylinders (left and right of midspan) at each point is considered. Thus, the calculation assumes that there are four sets of two concentrated loads on either end of midspan.

$$\delta = \sum_{i=1}^{4} \left(\frac{P_i * a_i}{24 * E * I} * (3 * L^2 - 4 * a_i^2) \right) \qquad \text{(Equation 5.14)}$$

In Equation 5.14, P is the magnitude of the average point load at each point, a is the distance from the end of the specimen to the point of the load, L is the total length of the beam, E is the modulus of elasticity, I is the moment of inertia, and δ is the deflection at midspan. When determining the fully-composite deflection, the modulus of elasticity of the wood poles is used with the moment of inertia of the whole transformed section of the beam. When determining the non-composite deflection, the modulus of elasticity of the wood is used with the sum of the moment of inertia of the wood and concrete layers in the transformed section. The resulting non-composite and fully-composite deflection values are 0.4322 in. and 0.0959 in., respectively. The resulting composite efficiency of Specimen M1 is 98.87%.

Specimen M2 was also ramp loaded at a time of 29 days with a 10.65 kip point load applied at midspan. The measured deflection was 0.302 in. Using Equation 5.15, the ordinary flexural formula for a simply supported beam subjected to a point load applied at midspan, the theoretical fully-composite and non-composite deflections can be calculated.

$$\delta = \frac{P * L^3}{48 * E * I} \qquad \text{(Equation 5.15)}$$

In Equation 5.15, P is the magnitude of the point load, L is the clear span of the beam, E is the modulus of elasticity of the wood poles, and I is the moment of inertia. When calculating the non-composite deflection, the moment of inertia is the sum of the moment of inertia of the two layers of the transformed section. When calculating the fully-composite deflection of the beam, the moment of inertia is calculated for the whole transformed section of the beam. Based on Equation 5.15, the theoretical fully-composite deflection and non-composite deflection are 0.316 in. and 1.399 in., respectively. This results in a composite efficiency of 101.3%, which is not possible. There are several potential sources of error that could contribute to the efficiency being above 100%.

There may be some error in the measurement of the deflection or load from the ramp load test. However, before testing, the accuracy of both the load cell and the string potentiometers were checked. There should be very little error from these sources. Another possible source of error is the effect of the environment on the specimen. As the temperature and humidity change, the behavior of the beam can change. As shown in Figure, 5.2b, the humidity during the last 8 days of the 28-day concrete curing period steadily decreased while the temperature steadily increased over the same period. This could result in a stiffer section, as the modulus of elasticity of the wood was determined experimentally several days before placing the concrete. Therefore, the theoretical deflection calculations may not accurately reflect the stiffness of the composite section, which could contribute to the calculated efficiency exceeding 100%, as discussed below.

The most likely source of error is in the cross sectional properties used to calculate the theoretical values. The utility poles are tapered and placed in opposite directions, and in LeBorgne's design procedure the moment of inertia is determined from the average diameter of the poles at midspan. In practice, the moment of inertia varies along the length of the poles. Figure 5.9 below provides a plot of the approximate variation in moment of inertia along the length of the poles. It is evident that there is significant variation in the moment of inertia along the length of the wood poles. The minimum value for the moment of inertia is at midspan (point C in Figure 5.9). The largest variation of the moment of inertia is 10.7%, which reflects the difference between point C and point E in Figure 5.9. Over the middle half of the beam, the largest variation in the moment of inertia is 2.3% (between points C and D in Figure 5.9). Since the variation in the moment of inertia over most of the beam is small, using the assumed value from midspan as a constant over the length is a reasonable approximation for the moment of inertia of the poles.

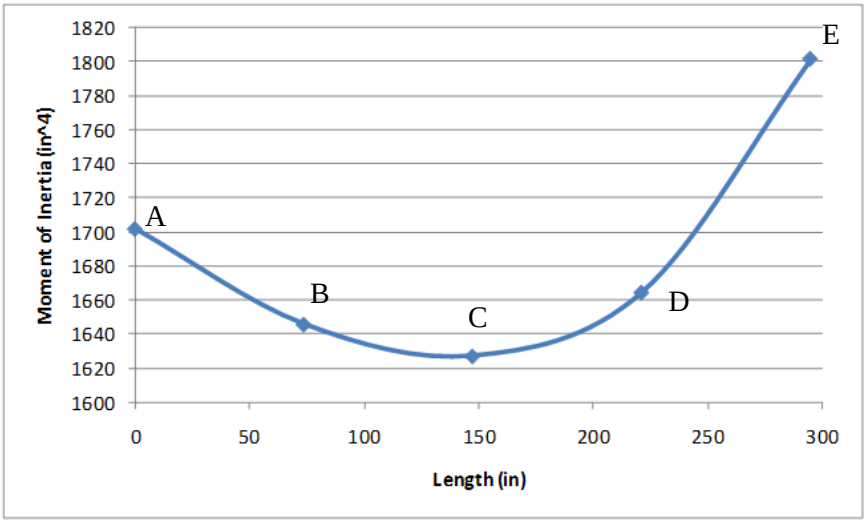

Figure 5.9 Variation in Moment of Inertia of Pair of Poles

Another consideration is the design method used by LeBorgne, from which the cross-sectional properties were originally calculated, assumes a cracked (concrete layer) transformed section. The resulting cross section is shown in Figure 5.10. This assumption implies that all concrete below the neutral axis (the hatched area) is cracked and is not considered in the analysis.

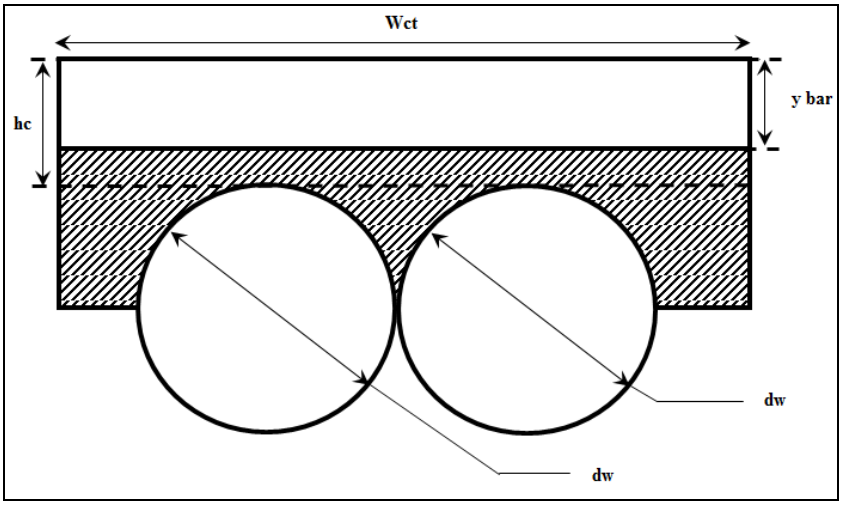

Figure 5.10 Cracked Transformed Section[4]

As plain concrete actually has some low tensile strength capacity, not all of the concrete below the neutral axis is actually cracked. The uncracked portion provides additional stiffness to the beam that was not accounted for in the preceding calculations. That step is reflected in the efficiency value calculated. Since it is unknown how much of the section may have cracked under the applied loads, it is useful to recalculate the entire concrete cross section assuming it is uncracked and include it in the transformed section.

The actual cross section is depicted in Figure 5.11. Based on the ratio of the moduli of elasticity of wood and concrete, the transformed section is determined. To account for the complicated geometry in the region of the cross section where the concrete is present below the crest of the round poles, an approximation is utilized. To account for this area of concrete, the transformed concrete section is

approximated by a linear change in width from the crest of the poles to the bottom of the concrete. The modified transformed section is shown in Figure 5.12. This approximation varies slightly from the actual geometry due to the circular poles; however, the differences are small. This additional area is also very near the centroid of the cross section and has only a small contribution to the moment of inertia.

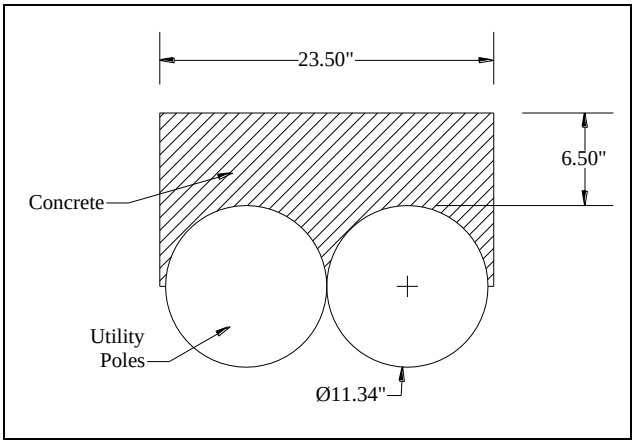

Figure 5.11 Actual Cross Section of Specimen M2

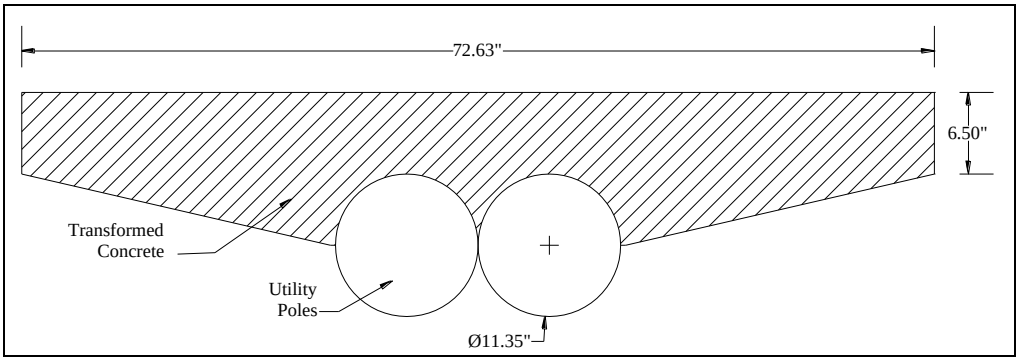

Figure 5.12 Modified Transformed Section of Specimen M2

Based on Figure 5.12, the section properties for determining the theoretical fully-composite and non-composite deflection were recalculated. The same procedure was also used for Specimen M1, as it is also likely that the section did not crack in that specimen either. Equations 5.14 and 5.15 are again used for calculating the composite efficiencies of Specimens M1 and M2, respectively, as indicated in Table 5.9. The results are 96.1% and 98.1% for Specimens M1 and M2, respectively, as compared with the previous values of 98.9% and 101.5%, respectively. The resulting composite efficiencies are very high, which is consistent with the findings of LeBorgne.[4,5] However, if the above cracked transformed section is considered, LeBorgne's values may be slightly lower than he reported. If only a portion of the concrete cracked, the EFF values would be in between the bounds determined above.

Table 5.9 Revised Composite Efficiency Calculations

		Specimen M1	Specimen M2
Non-Composite	*L*	295 in	295 in
	E	1905000 psi	1238000 psi
	I	3566.0 in^4	6695.3 in^4
	Δ	0.262 in	0.687 in
Fully Composite	*L*	295 in	295 in
	E	1905000 psi	1238000 psi
	I	10051.1 in^4	15614.8 in^4
	Δ	0.096 in	0.295 in
Actual Deflection	Δ	0.010 in	0.302 in
Composite Efficiency		**96.10%**	**98.10%**

5.3 Repeated Load Tests

After the 28-day concrete curing period, Specimen M2 was subjected to repeated loads using the testing protocol described in section 4. The stiffness of the specimen and any changes in the permanent deflection were monitored at various times throughout the load cycling. The stiffness was measured by performing ramp load tests to approximately 10 kips. From a plot of the load vs. deflection, the effective stiffness was determined by using the slope of a line fit to the load-deflection data. "Effective stiffness" has been used by others as an indication of the stiffness of the beam.[2,3] From here forward, the effective stiffness will be referred to as either "EI" or "effective stiffness" interchangeably. The value of EI for the partially composite section is calculated from the ordinary flexural equation for a simply supported beam with a point load at midspan as shown in Equation 5.16, namely,

$$EI = \frac{P}{\Delta} * \frac{L^3}{48} \qquad \text{(Equation 5.16)}$$

In the equation, *EI* is the effective stiffness of the specimen, $\frac{P}{\Delta}$ is the slope of the linear fit to the load versus deflection data over the course of the ramp load test, and *L* is the span of the beam. Plots of the load versus deflection for all ramp load tests included in the testing are provided in the thesis produced from this work.[38] The results for the changes in EI are reported subsequently.

Before any load cycles were applied, an initial ramp load test was performed to determine the baseline EI. After subsequent loadings, the calculated EI values were compared to the initial value. The EI after various numbers of cycles is reported below as a percentage of the initial value. This provides a very useful indication of the stiffness over time.

Changes in the overall deflection of the beam were also monitored. However, there are a number of complications to using this measurement as a basis of assessment of durability. First, the cycles of load were applied over an extended period of several weeks in sets of 2,500 or 5,000 cycles. A maximum of 5,000 cycles were applied on any given day of testing. An unavoidable consequence is that rheological phenomena also occurred during the test, resulting in time-dependent deflections under the dead load of the beam itself. During testing, there is always some amount of load on the beam as the load fluctuates

from approximately 0.5 kips to 10.5 kips. In addition, under the testing frequency, it takes about 5.5 hours to perform 5,000 load cycles. Creep deflections likely occur due to the overall load duration of the repeated loading. Thus, any analysis using the permanent deflection data must be considered in light of those factors.

Changes in EI occur over time. For the first 15,000 cycles, the EI value was determined after sets of 2,500 cycles. The frequency of checking EI was decreased to every 5,000 cycles for the remainder of the cycles, up to 35,000 cycles. This was done to speed the process of the repeated loading. Also, it was determined from the trend that the value of EI was not needed after every 2,500 cycles. The results from this testing are listed in Table 5.10 and shown in Figure 5.13. In the table, the "Test Conditions" column contains the number of cycles that had been completed as well as the age of the concrete in parentheses. Note that the repeated load testing took place over a period of 7 weeks after the 28-day curing period of the concrete.

Table 5.10 Changes in EI Over the Course of the Repeated Loads

Test Conditions	Cycles	P/delta (kip/in)	EI (kip-ft^2)	% Initial EI
Initial Stiffness (29 days)	0	34.775	10763	100.0%
Before Cyclic Loads(33 days)	1	34.188	10582	98.3%
After 2500 Cycles (34 days)	2500	34.195	10584	98.3%
After 5000 Cycles (35 days)	5000	34.017	10529	97.8%
After 7500 Cycles (35 days)	7500	34.029	10532	97.9%
After 10000 Cycles (37 days)	10000	33.772	10453	97.1%
After 12500 Cycles (37 days)	12500	33.588	10396	96.6%
Before 12500-15000 (49 days)	12500	33.802	10462	97.2%
After 15000 Cycles (49 days)	15000	33.796	10460	97.2%
After 20000 Cycles (50 days)	20000	33.589	10396	96.6%
After 25000 Cycles (51 days)	25000	33.479	10362	96.3%
Before 25000-30000 (75 days)	25000	32.999	10214	94.9%
After 30000 Cycles (75 days)	30000	32.389	10025	93.1%
After 35000 Cycles (76 days)	35000	32.883	10178	94.6%

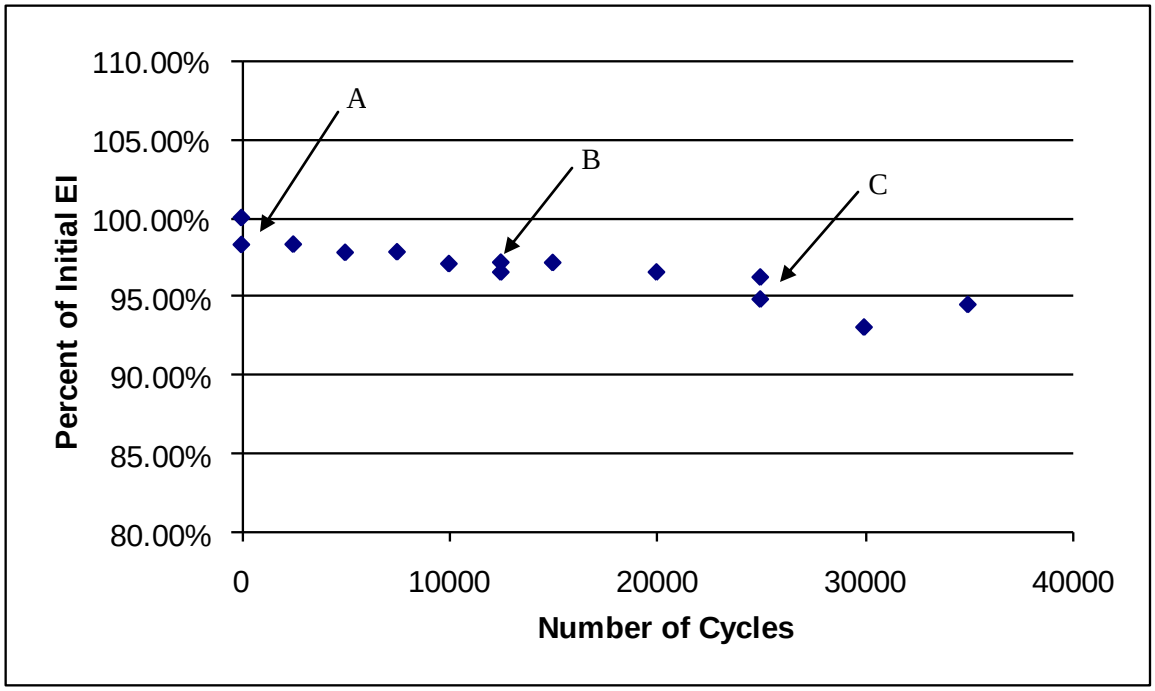

Figure 5.13 Specimen M2 EI Variation Throughout Repeated Load Testing

Several observations can be made from the data shown in Table 5.10 and Figure 5.13. First, there are several points of interest labeled on Figure 5.13. Point A corresponds to the point that is labeled in Table 5.10 as "Before Cyclic Loads." The initial stiffness test was performed on the day 29 of concrete curing so that the stiffness test would correspond with the 28-day tests of the concrete test cylinders. However, due to schedule constraints, the repeated loading itself began on the day 34. Thus, an additional stiffness test was done the day before the repeated tests began. Therefore, the listed difference in EI is not the result of degradation from the loading, but rather a more general variation in the experimentally measured values. One additional oversight in the data for point A is that only one ramp load was performed at that time. For all other effective stiffness tests, the ramp load was applied multiple times (usually two, sometimes three) in order to establish the repeatability of the data.

All points between point A and B on Figure 5.13 correspond to ramp load tests after sets of 2,500 repeated load cycles, with no more than two days between data points. After 12,500 cycles were performed, there was a break in the testing for several days. This break in the data is represented as point B. After the 12,500 cycles had been completed, a ramp load test was done to measure the EI. This is the lower data point at point B. Before resuming testing, an additional stiffness test was done to determine the starting point of EI after the 12-day period between tests. The small increase in the EI (0.6%) is somewhat to be expected, as the strength of concrete is known to vary with time. Equation 5.17 provides the variation of strength for Type I moist cured concrete.[39] As the strength increases, the stiffness also increases as it is related to the strength of concrete as described by Equation 5.18.[39]

$$f'_{ct} = \frac{t}{4.00 + 0.85t} * f'_{c} \qquad \text{(Equation 5.17)}$$

$$E_{ct} = 57000 * \sqrt{f'_{ct}} \qquad \text{(Equation 5.18)}$$

In these equations, E_{ct} is the modulus of elasticity (psi) of the concrete at time t, f'_{ct} is the compressive strength (psi) of normal weight concrete at time t, and f'_{c} is the compressive strength (psi) of concrete at 28 days. Based on the time dependence of the stiffness of concrete, the increase in EI of the specimen at point B is not surprising. Equations 5.17 and 5.18 predict that the modulus of elasticity of the concrete layer would increase 1.4% over the 12-day period, while it is assumed that the modulus of elasticity of the wood layer did not change over the period. Thus, the increase in EI of the specimen observed (0.6%) seems very reasonable.

Point C in Figure 5.13 is similar to point B and corresponds to a 24-day break in the testing after 25,000 load cycles. In this case, there was a drop in the EI over the time. The upper point corresponds to the load test immediately after completing 25,000 load cycles with a concrete age of 51 days while the lower point corresponds to the strength 24 days later with a concrete age of 75 days. The decrease in EI (1.3%) over time observed is not expected, as Equations 5.17 and 5.18 predict an increase in the modulus of elasticity of the concrete layer of 1.4% during the 24-day period. However, it is possible that this decrease is related to the rheological phenomena taking place and the environmental exposure conditions. Some micro-failure or slip may also have occurred during this period.

Figure 5.14 provides the temperature and relative humidity data from the time that Specimen M2 was cast until the repeated load tests were completed. It is difficult to draw any conclusions as to the decrease in EI at Point C based on the temperature and humidity data. However, there is a 10°C increase in the temperature between the 54th and 72nd days of testing. During the same period, there is a decrease in the relative humidity of approximately 10%. These changes in the environmental conditions can have a noticeable effect on the behavior of the beam. Also, on the day 54, there is a significant drop in the temperature and corresponding jump in the relative humidity. A sudden change in the environmental conditions could also affect the behavior of the beam, especially as it relates to changes in temperature. In his research, To[17] observed that the temperature of the composite section closely follows that of the ambient environment, but changes in relative humidity have a smaller, delayed effect as a result of the diffusion process. The cause of the change in EI at point C in Figure 5.14 is unclear, but it is likely a result of the rheological phenomena occurring throughout the repeated load testing.

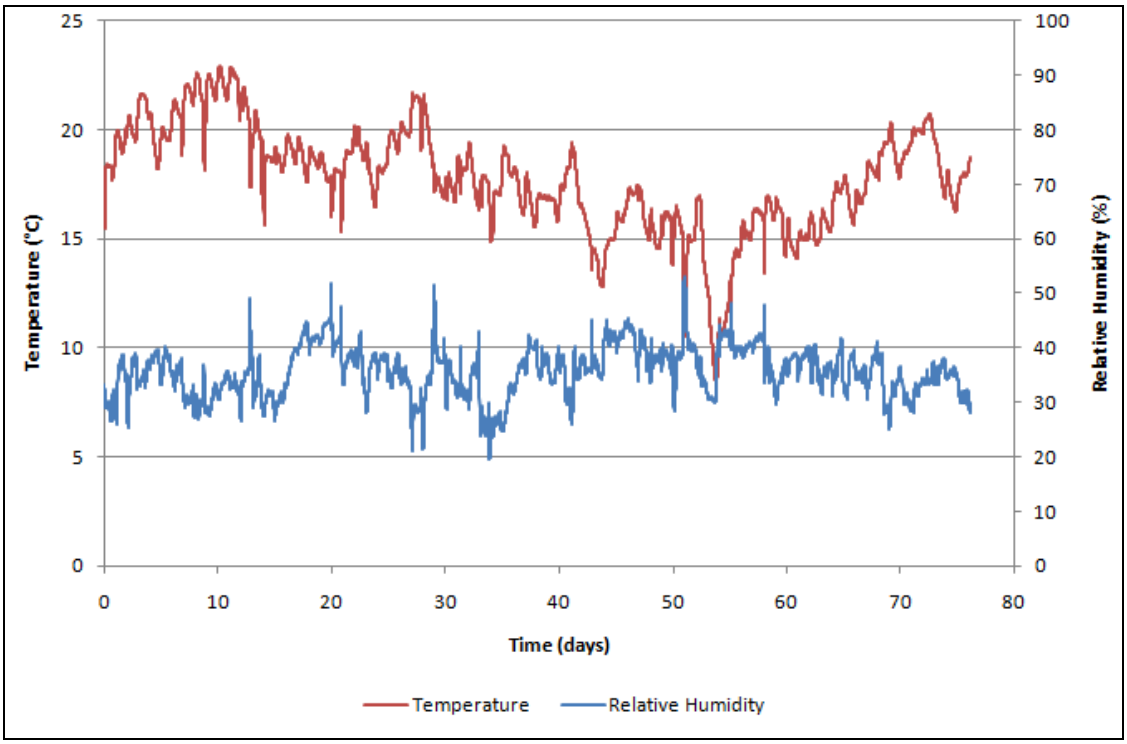

Figure 5.14 Specimen M2 Temperature and Relative Humidity Data

Overall, the set of data in Figure 5.13 indicates that small decreases in EI occurred over time. The final EI after 35,000 cycles is approximately 5.5% lower than the initial effective stiffness. This decrease in EI is very small as compared with Fast's research in this area. Fast[2,3] conducted a durability study on a set of replicated wood-concrete composite beams comprised of dimension lumber for the wood layer. His study included repeated load tests to 21,600 cycles with the EI of the beams measured before and after the load cycles.

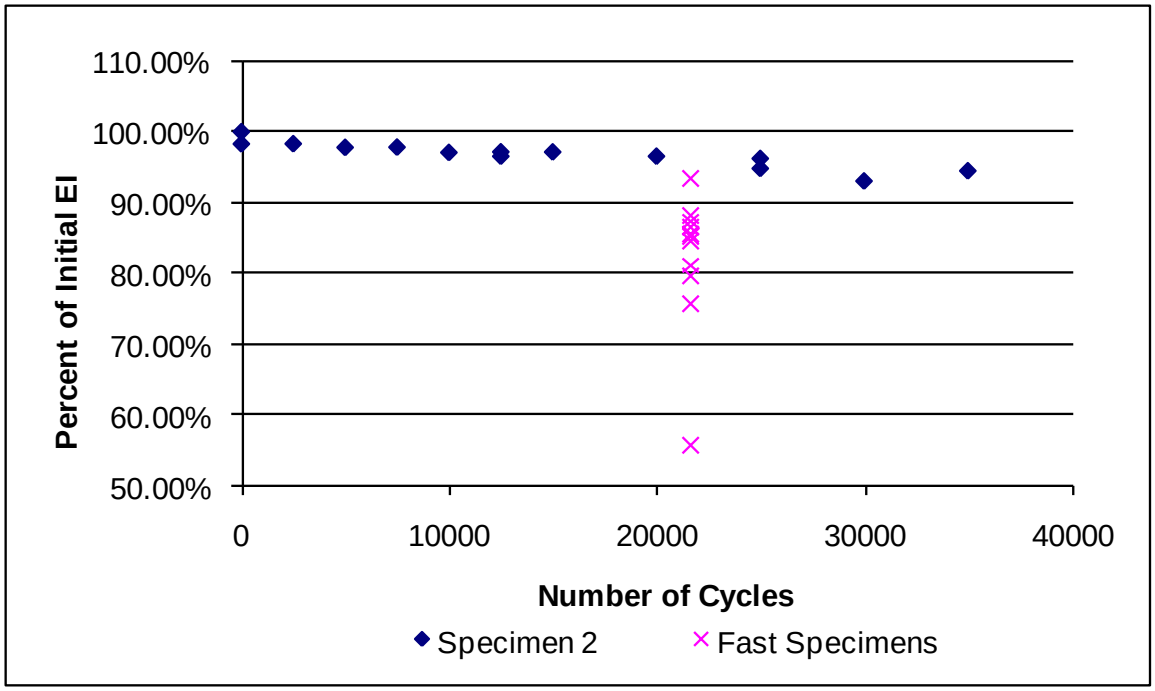

Figure 5.15 Repeated Load Test Results from Specimen M2 and Fast

Figure 5.15 shows the data Fast obtained from his study as compared to the data from this study. Fast's research included 11 repeated load specimens. The X's on the plot represent the results of each specimen. The average decrease was 17.73%. The highest point on the plot had a decrease of 6.35% after 21,600 cycles. The lowest point represents a decrease of 44.14% of the initial EI, but again, is an outlyer. Clearly, Specimen M2 performed better than any of the specimens in Fast's study and much better than the average. Based on LeBorgne et al.,[21] the quality of the concrete mix and the construction procedures for the composite beams have been dramatically improved since those used by Fast and are believed to have led to the much improved results herein.

At the end of the testing, 35,000 cycles, the general trend of the EI data as a function of cycles is still downward. Additional decreases should be quite small, as the stiffness of the specimen decreased quite slowly and even showed an increase in stiffness between 30,000 cycles and 35,000 cycles. Since the decreases were small and there was some possible damage occurring to the hydraulic actuator used to load the specimen, the testing was stopped.

Another aspect in the repeated load testing is possible non-recoverable deflection of the beam that would indicate some sort of micro-failures or slip occurring during the repeated load testing. Such non-recoverable deflection can result from the physical degradation of the beam. Any degradation of the notched connection would reduce the degree of composite action in the beam. To monitor changes in deflection, the vertical deflection of the specimen at midspan was recorded before and after each set of load cycles applied to the specimen. The average deflection of the end supports was subtracted to remove the effect of any vertical movement of the supports. The deflection was monitored before and after each set of repeated loads, noting changes. Table 5.11 lists the corrected midspan deflection of the specimen before and after each set of loads, the incremental deflection of the specimen during that specific test, and the cumulative incremental deflection of the beam over the duration of the testing. For example, before any of the cyclic loads were applied, an initial ramp load test was done to determine the initial stiffness of the specimen. Before the ramp load was applied, the deflection of the beam was 1.311 in. Then the ramp load was applied and removed. After the load was removed the deflection was 1.335 in. The difference

in the deflection values provides the incremental non-recoverable deflection due to the ramp load, 0.024 in. The same measurements were taken before and after each set of load cycles were applied, and the results are provided in Table 5.11.

Table 5.11 Non-Recoverable Deflection During Repeated Load Tests

Test		Deflection (in)	Incremental Deflection (in)	Cumulative Incremental Deflection (in)
Initial Stiffness	Before	1.311	0.024	0.024
	After	1.335		
0-2500	Before	1.342	0.014	0.038
	After	1.356		
2500-5000	Before	1.350	0.002	0.040
	After	1.352		
5000-7500	Before	1.352	0.002	0.042
	After	1.354		
7500-10000	Before	1.356	0.014	0.056
	After	1.370		
10000-12500	Before	1.370	0.001	0.057
	After	1.371		
12500-15000	Before	1.404	0.022	0.079
	After	1.426		
15000-20000	Before	1.419	0.007	0.086
	After	1.426		
20000-25000	Before	1.429	0.016	0.102
	After	1.445		
25000-30000	Before	1.443	0.010	0.112
	After	1.453		
30000-35000	Before	1.454	0.005	0.117
	After	1.459		

The data in Table 5.11 indicate erratic values for the incremental deflection (column 4) occurred throughout the testing; however, the average incremental deflection was 0.011 inch over the increments of repeated loads. This increasing deflection is primarily attributed to the rheological effects occurring simultaneously with the repeated load tests. During the repeated load tests, the specimen is still subject to changing temperature and humidity that may have an impact on the deflection response. The largest value for the incremental deflection is 0.024 in., which occurred during the initial stiffness test (a series of ramp load tests). It is logical that this would be the largest value, as the specimen may settle somewhat as it is loaded for the first time. The variation in the other incremental deflection values may in part be due to the rheological effects taking place throughout the testing. As the temperature and relative humidity of the environment change, the deflection of the specimen also changes. Thus, it is not possible to distinguish what portion of the deflection pattern is a result of the degradation of the notched connection from the portion that occurs as a result of the rheological effects.

The cumulative incremental deflection at the end of 35,000 load cycles was 0.117 in., which is modest. It constitutes only 8% of the total deflection of the beam (1.459 in.) measured immediately after the 35,000 cycles were completed. Figure 5.16 is a plot of the cumulative deflection versus the number of load cycles completed. It displays the variation in the deflection that was seen throughout the testing. The increases in the deflection are nearly linear over the testing period; however, it does appear that the trend in the data is starting to slightly decrease near the end of the data set. Since the time-dependent effects

cannot be separated from the effect of the load cycles, the change in EI is a more dependable indication of the durability of Specimen M2 than the changes in permanent deflection.

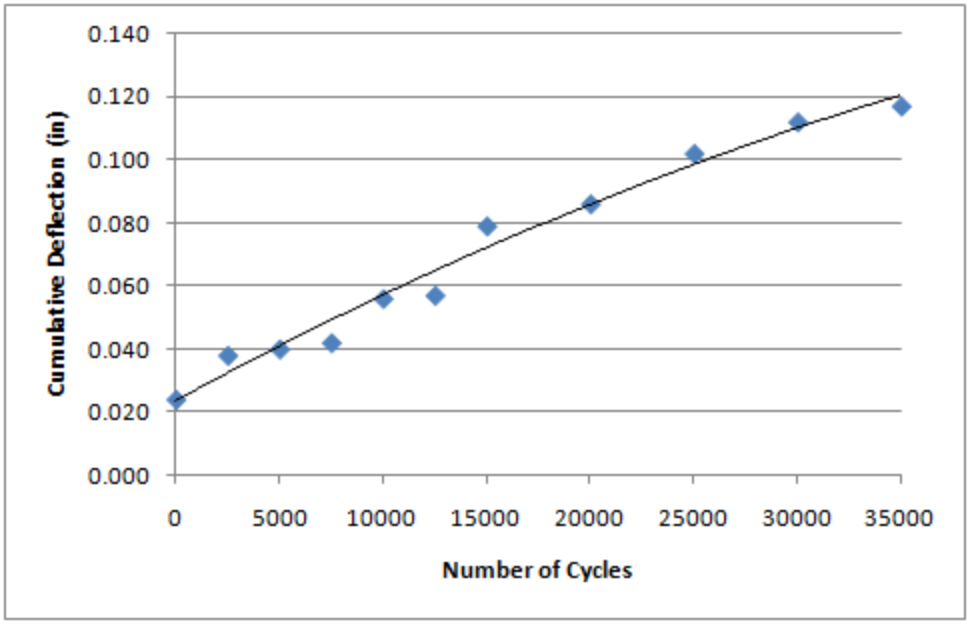

Figure 5.16 Cumulative Deflection throughout Repeated Testing

After the 35,000 cycles were completed, a final ramp load test was performed. In that final test, there was a deflection of 0.320 in. at an applied load of 10.66 kips. With this applied load, the theoretical non-composite deflection is 0.688 in. and the fully-composite deflection is 0.295 in. This results in a composite efficiency of 93.6%. The initial composite efficiency for this specimen was 98.1%. The observed decrease was 4.5%, which is small. The notched connection appears to have been very durable under the 35,000 cycles of repeated loading.

6.4 Long-Term Creep Analysis

Long-term creep was monitored experimentally with Specimen M1. This test is ongoing with the first 256 days of the testing considered herein. A permanent live load was applied after the 28-day concrete curing period. Figure 5.17 shows the measured total deflection as it varied over time, including the data for each pole separately and the average of the two pole deflections.

Table 5.12 contains a summary of the deflections observed as a percentage of the total deflection. In the table, "Percent of Maximum Deflection" is calculated as the incremental deflection divided by the total long-term deflection (1.748 in.) at 256 days. It is clear that time-dependent deflections constituted a significant component of the total deflection observed throughout the testing.

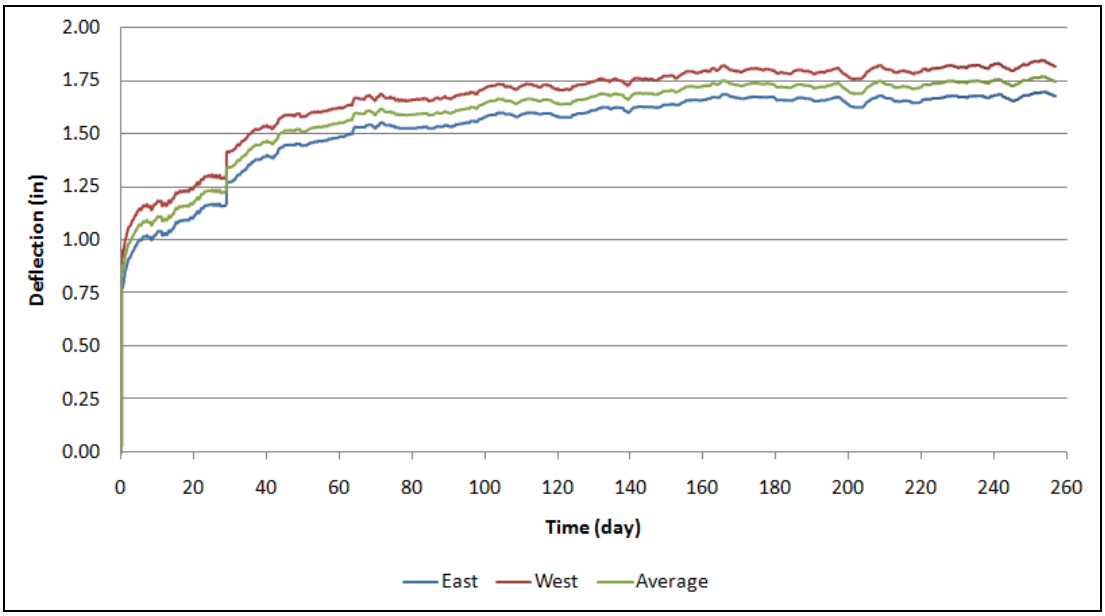

Figure 5.17 Midspan Deflection Data for Specimen M1

Table 5.12 Summary of Deflection for Specimen M1

Event	Total Deflection(in)	Incremental Deflection (in)	Percent of Maximum Deflection
Dead Load Application	0.746	0.746	42.67%
28-day Deflection	1.241	0.495	28.32%
Live Load Application	1.341	0.100	5.72%
Long Term Deflection (256 days)	1.748	0.407	23.28%

The concept of a "creep coefficient" (as used earlier in Equation 2.4) is a common way of quantifying the deflection due to creep. This coefficient is the ratio between the time-dependent deflection and the short-term deflection, as expressed by Equation 5.19,

$$\phi_C = \frac{\Delta_T - \Delta_E}{\Delta_E} \qquad \text{(Equation 5.19)}$$

where ϕ_C is the creep coefficient, Δ_T is the total deflection, and Δ_E is the short-term deflection due to an applied load.

For the wood-concrete composite beam, ϕ_C is a difficult quantity to define. During the first 28 days, the properties of the concrete layer are changing significantly. Therefore, the creep coefficient could be considered in two primary ways. First, the live load could be considered by itself. In this case, the assumption is made that all time-dependent deflection that occurs after the live load application is due to the live load. However, this is not the case. After the live load is applied, the specimen continues to also experience time-dependent deflections due to its dead load. Therefore, another method of quantifying the creep coefficient is to consider the total deflection (1.748 in.) and the sum of all elastic deflections (0.846 in.). By including the short-term deflection due to the dead load, the creep coefficient will consider the time-dependent deflection which results from both the dead and the applied live load. When the live load is considered separately, the short-term deflection is 0.100 in. and the total deflection is 0.507 in.,

resulting in a creep coefficient for the 256-day experimental period of 4.07. However, when the total short-term deflection is included, the creep coefficient is only 1.07. Since the total short-term deflection method seems to better represent the time-dependent behavior, it has been used subsequently when considering the creep coefficient.

The data in Figure 5.17 represents the midspan vertical deflection of the specimen (minus the average of the two end span deflections) over time. The adjustment removes any deflection that may result from vertical movement of the end supports or the specimen settling into the end supports. During the test, it was necessary to remove the string potentiometers that measured the end span deflections after approximately 84 days so that they could be used for other research activities. This disturbance appears to be insignificant as the monitored deflection at the end supports was essentially unchanged for many days prior to their removal (see Figure 5.18). For all times after the string potentiometers were removed, the end support deflection was assumed the same as it had been at the time of their removal.

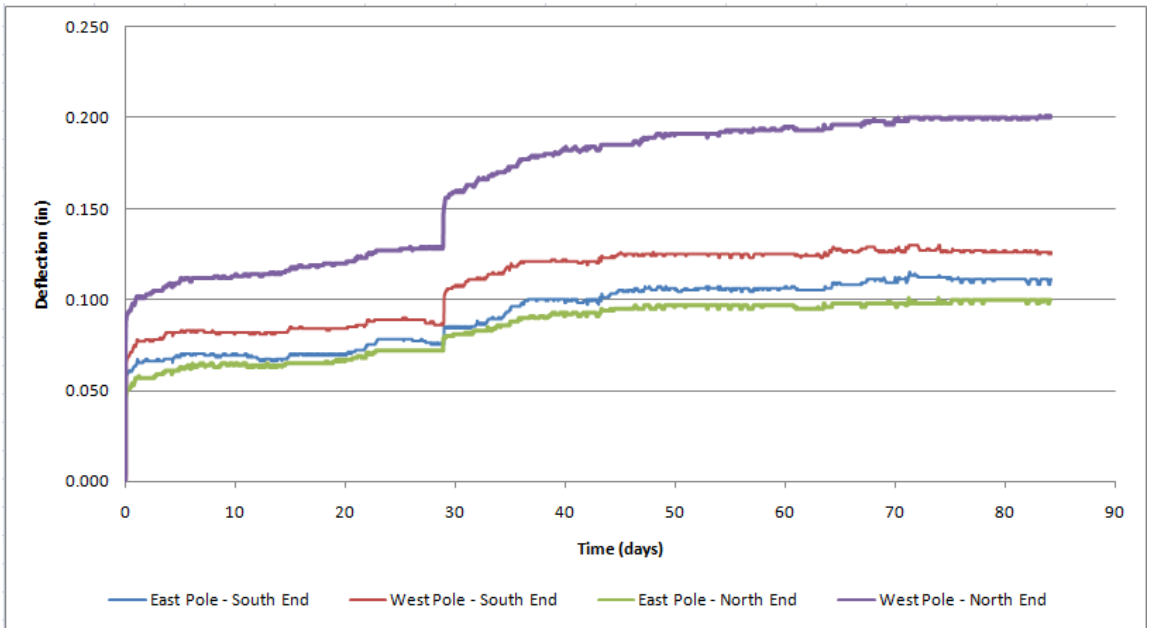

Figure 5.18 End Support Deflections for Specimen M1

Figure 5.19 illustrates the slip (horizontal interlayer relative displacement) data recorded throughout the load testing. The negative slip values reflect the concrete "shortening" relative to the wood, or conversely the wood "lengthening" relative to the concrete. Some disruption occurred in the slip measurement. The dial gage on the south end of the beam became detached from the specimen 45 days into the test. It was reattached and the measurement was corrected to match the slip before the gage fell off. Any slip that occurred during the time that the gage was not attached was not included in the measurement. On the day 218, the gage on the south end was bumped, and the measurement was corrected again. These two inconsistencies in the data appear to have had little impact on the overall results as the behavior of the north and south ends are still generally continuous without any obvious changes. In general, the slip behavior is very similar on each end of the specimen for the first 120 days. After that point, the slip on the south end increases at a slightly faster rate than the slip on the south end of the specimen. The observed divergence between the slip deflections at the ends of the specimen could be due to some sort of micro failure occurring in the regions of the notches.

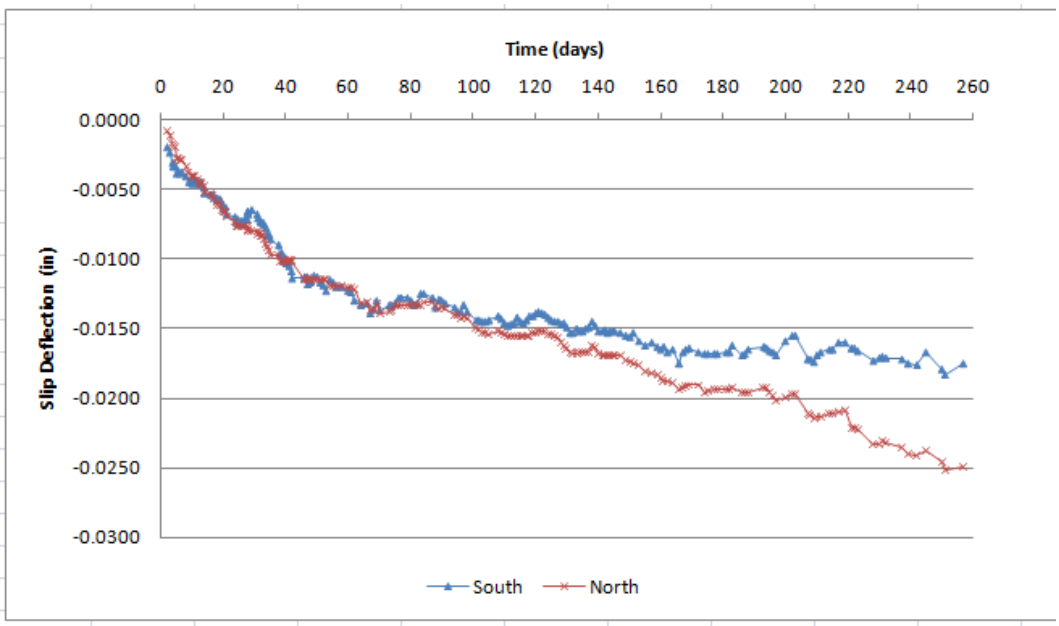

Figure 5.19 Slip Deflection at End Supports of Specimen M1

Two other significant trends are evident in Figures 5.17 through 5.19. The first occurs on the day 28 when the live load was applied to the specimen. In Figure 5.17 and Figure 5.18, a sudden increase in the vertical deflection of the specimen occurs both at midspan and at the ends of the specimen. No apparent sudden increase in interlayer slip occurs at this point, which indicates that the notched connection provides high composite action as there was little measureable slip between the layers. The other observation is that the slip measured on the north end of the specimen was larger than the slip on the south end. Due to a large overhead garage door near the south end of the specimen, the temperature and humidity at each end may have been noticeably different, resulting in the different rates of interlayer slip observed after day 120.

One of the goals of the research was to predict the long-term deflection of the composite beam using a numerical model. Fragiacomo's[5] 1D finite element software program was used for this purpose. The software input consists of the details of the cross section and length of the specimen, the material properties, the interlayer connection, the slip modulus, the loading history, a temperature and humidity record, etc. The "slip modulus" is the slope of the load vs. slip plot obtained in a push out test ("slip test"). The temperature and humidity record used was that measured during the duration of the testing.

The software assumes a rectangular cross section, but the specimens in this study were constructed with round poles. Therefore, the round cross section was approximated by a rectangular section. There are several factors to consider in this transformation. Although the perimeter and volume are important factors in determining the moisture content and other parameters in the program, it was decided that the stiffness is the more important parameter. Thus, the rectangular cross section was modified to reflect that. The cross section of the poles in the modified cross section was configured to have the same local centroidal moment of inertia as that of the actual round poles. The depth of the rectangular concrete layer was set so that the modified beam's cross section had the same transformed section moment of inertia as the actual transformed cross section. The resulting approximation is shown in Figure 5.20.

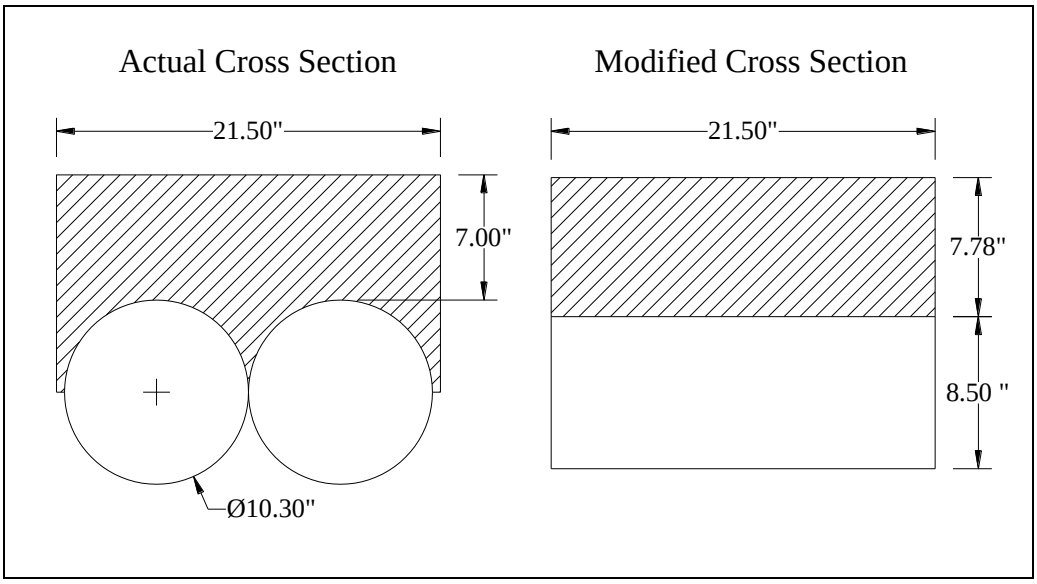

Figure 5.20 Modified Cross Section Used for FE Model

The software program was initially executed using Toratti's linear model for timber behavior, the CEB-FIP Model Code 90 prediction of concrete creep, and the ACI 209-92 prediction of concrete shrinkage. The dimensions and material properties for Specimen M1 were input. The plotted results are shown in Figure 5.21. The resulting prediction underestimated the short-term deflection, overestimated the trend in the long-term deflection, and overestimated the deflection due to the application of the live load at 28 days. Consequently, adjustments to the model were made to account for each of these inconsistencies.

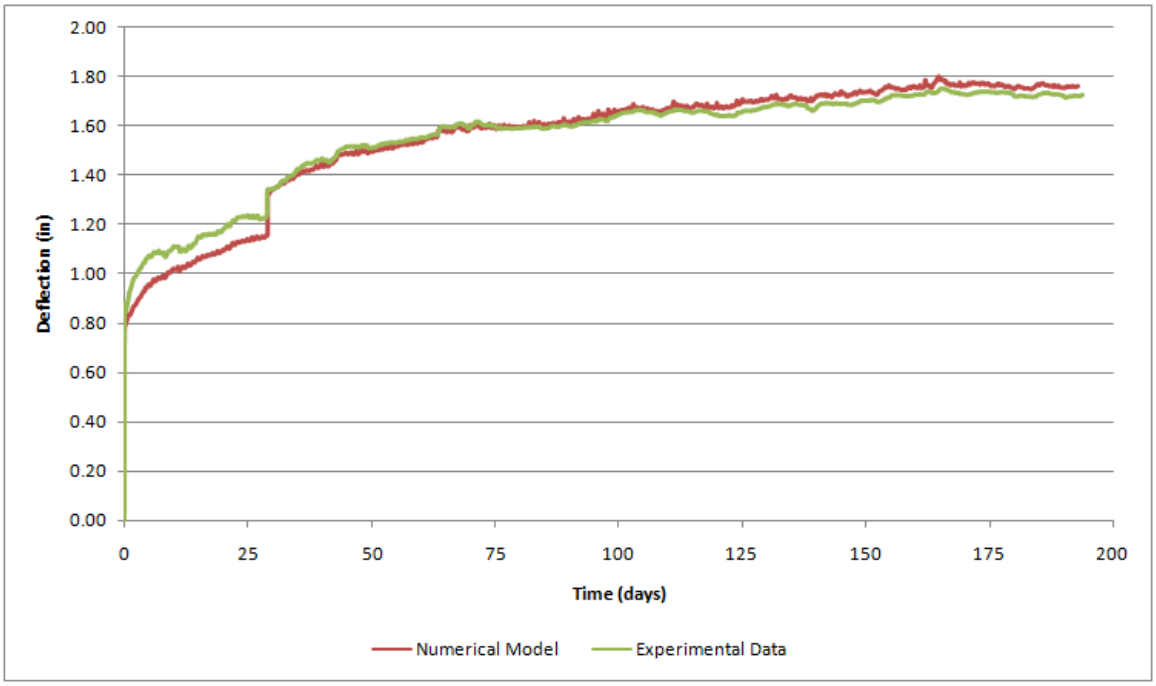

Figure 5.21 Experimental Data Compared to Initial FE Model

The slip modulus is a measure of the overall stiffness of the notched connection at the interface of the two layers. The value initially used in the numerical model was (892 kip/in.) a value determined experimentally by Fast et al.[33] for his smaller specimens constructed with dimension lumber. To account for the much larger bearing area for the notch in the utility poles, the slip modulus was increased by a ratio of the cross sectional area of the notch in the utility poles and the cross sectional area of the notch in Fast's dimension lumber layer. That ratio is 4.765. The resulting slip modulus was 4250 kip/in., a significant increase. Consequently, the short-term deflection predicted at the time of live load application was reduced, which provides better agreement between the model and the experimental data.

Next, the long-term trend in the deflection was considered, and it was rationalized that the shrinkage function used was the probable cause of the observed error. The FE model employs the ACI 209-92 formulation for the shrinkage function. Specifically, the strain due to shrinkage is given by,

$$(\varepsilon_{sh})_t = \frac{t}{35+t} * (\varepsilon_{sh})_u \qquad \text{(Equation 5.20)}$$

where $(\varepsilon_{sh})_t$ is the shrinkage strain at time t and $(\varepsilon_{sh})_u$ is the ultimate shrinkage strain as expressed by,

$$(\varepsilon_{sh})_u = .000780 * \gamma_{sh} \qquad \text{(Equation 5.21)}$$

where γ_{sh} is a correction factor composed of several different adjustments. One of the adjustment factors considers the ratio of volume to surface area of the concrete section. The shrinkage function initially used in the program included the smaller cross-section of the beam constructed from dimension lumber. To account for the larger cross section, a correction factor was modified. The correction factor, γ, is expressed as,

$$\gamma = 1.2 * \exp\left(-0.12 * \frac{V}{S}\right) \qquad \text{(Equation 5.22)}$$

where $\frac{V}{S}$ is the ratio of volume to surface area of the concrete layer. For the beams studied herein, the shrinkage function used in the software needed to be multiplied by a factor of 0.706. This correction reduces the deflection due to shrinkage which should provide increased agreement between the model and the experimental data.

The rate of deflection at the beginning of the test period differed for the initial FE model and the data. This difference is attributed to an increase in the temperature of the concrete layer as it began to cure. It has been shown that the temperature of the concrete layer can increase 15-30°C during the first 12-15 hours of curing and that the cooling period can last 150-180 hours thereafter[36]. However, this can vary depending upon variables such as the type of concrete, the geometry of the concrete section, and the ambient environmental conditions. To account for this, the temperature data applied to the model were modified. It was assumed within the model that the concrete began to gain significant strength 6 hours after being placed. To correspond with this, the temperature at that point in time was increased by 15°C. Then the temperature was decreased linearly over a period of 24 hours to the actual ambient temperature. These values are less than the values cited in the literature[36]; however, it was reasoned that the concrete portion of this beam specimen is likely much smaller than that of the steel-concrete composite bridges that are considered in the literature. With a smaller cross-section, the concrete would cool faster and likely experience less increase in temperature. Regardless, this assumption resulted in a good fit to the experimental data.

As a result of adjusting the slip modulus, the shrinkage function, and the temperature of the concrete layer, good agreement between the 1D finite element model and the experimental data has been achieved. Table 5.13 provides many of the important inputs for the program. The results of the revised model are shown in Figure 5.22.

Table 5.13 Program Inputs

Full Beam Width	21.50 in
Concrete Depth	7.78 in
Timber Depth	8.50 in
Number of Finite Elements	9
Layers of Concrete	20
Layers of Timber	50
Slip Modulus	4250 kip/in
Timber Modulus of Elasticity	1905000 psi
Concrete Modulus of Elasticity	3281300 psi
Concrete Compressive Strength	4.86 ksi

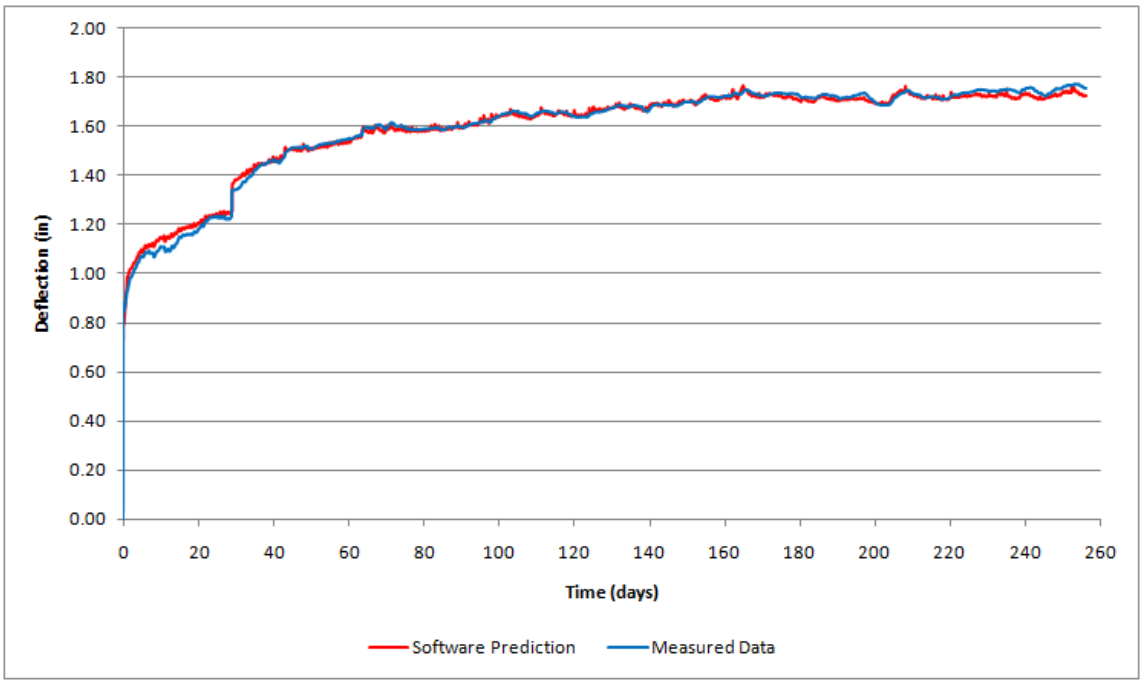

Figure 5.22 Experimental Deflection Data Compared to FE Model with Corrections

6. OBSERVATIONS AND CONCLUSIONS

6.1 Observations

The deflection of the unshored beams was monitored as the concrete was placed and during the curing period of the concrete. The approximately 1 in. of camber, which resulted from the tapered utility poles, was maintained through the placement of the concrete; however, by the end of the 28-day concrete curing period, the deflection due to the placement of the concrete as well as the time-dependent effects exceeded the initial camber by approximately 0.25 in. Significant time-dependent deflections during the 28-day concrete curing period were observed in the specimens. The deflections over this period were 28% - 65% of the short-term deflection due to the placement of the concrete.

To predict the deflections which would occur over the curing period, an empirical equation was developed from a curve fit to the data. The resulting equation (Equation 5.11) is a modified version of the equation previously developed by LeBorgne. LeBorgne's equation predicted the 28-day deflection of his two beams within 3% error; however, when applied to Specimens M1 and M2, the percentage error was approximately 10%. The modified equation (Equation 5.11) predicts the deflection of the four specimens, with errors less than 5% over the 28-day period, a significant improvement.

After the 28-day concrete curing period, a load was applied to each specimen, and the composite efficiencies were determined to be 96.1% and 98.1%. These values were determined utilizing theoretical fully-composite and non-composite deflections based on a transformed section of the composite beam that assumed that none of the concrete was cracked. This is in contrast to LeBorgne, who assumed that all concrete below the neutral axis of the beam was cracked and, therefore, was not included in the determination of the moment of inertia. When LeBorgne's method was used for the specimens in this study, the composite efficiency exceeded 100%. Therefore, it is likely that the composite efficiencies reported by LeBorgne are slightly overstated, as are those of Specimen M1 and Specimen M2, if the concrete partially cracking is considered.

The effect of repeated loads was an important consideration. For Specimen M2, the final effective stiffness (after 35,000 load cycles) was 94.6% of the initial effective stiffness. As the 35,000 load cycles were approached, the stiffness was still decreasing; however, the rate of decreasing stiffness appeared to be slowing. While the observed changes in stiffness are important factors to consider in design and construction of the composite beams, the changes were relatively small as compared with those observed by Fast. In Fast's tests to 21,600 load cycles, the average final effective stiffness was 82.3% of the initial value.

The time-dependent deflection was observed to be a large component of the overall deflection observed in the specimen. At the end of 256 days, with a permanent live load applied at 28 days, the time-dependent deflection was 51.6% of the total measured deflection (due to the dead and live load application as well as the time-dependent effects). Two methods were considered for determining the creep coefficient. First, the total deflection from the time of the application of the live load was considered. In this case, the short-term deflection was 0.100 in. and the total deflection was 0.507 in., resulting in a creep coefficient of 4.07. However, this method neglects the portion of the long-term deflection due to the dead load application that occurs after the live load application. The short-term deflection (from dead and live loads) was 0.846 in., and the total deflection was 1.748 in. This resulted in a creep coefficient of 1.07 at a time of 256 days.

It is important to be able to predict the long-term deflections as it pertains to serviceability considerations in design of the composite beam. The 1D finite element model developed by Fragiacomo was first used to predict the deflection during the 256-day experimental study. With appropriate assumptions and input, there was good agreement between the FE model and the experimental data.

6.2 Conclusions

- The empirical equation developed in this study (Equation 5.11) to predict the deflection of a wood-concrete composite beam during the 28-day concrete curing period improves upon the equation previously developed by LeBorgne. The new equation includes compensation for specimens with different spans.
- The assumption of the degree of cracking in the concrete layer is important in calculating the composite efficiency.
- Specimen M2 indicates the proposed beam system can withstand 35,000 load cycles at the design service load while losing only 5.4% of the initial effective stiffness.
- Specimen M2 also indicates that improvements to the specimen construction process, including adding a moisture sealant and changing the concrete mix design, has improved the quality and durability of the notched connection. The performance of Specimen M2 is significantly improved from a prior study of repeated loads conducted by Fast[2].
- Fragiacomo's one dimensional finite element model resulted in a very accurate prediction of the time-dependent deflection over the experimental 256-day period once adjustments were made to account for the effects associated with the larger geometry of the specimen as compared with the smaller specimens for which the model has previously been utilized.

7. REFERENCES

1. American Society of Civil Engineers. “Infrastructure Report Card 2005.” 2005. 14 January 2009. <http://www.asce.org/reportcard/2005/page.cfm?id=22>

2. Fast, Ryan. “Durability Studies of Layered Wood-Concrete Composite Connections and Beams.” Thesis. Colorado State University. 2003.

3. Gutkowski, R., Fast, R., Balogh, J., & Fragiacomo, M. (2006) “Time-Dependent Performance of Notched Wood-Concrete Composite Beams,” Proceedings, 11th International Conference and Exhibition in Structural Faults and Repair. Edinburgh, Scotland.

4. LeBorgne, Matthew. “Analysis of Wood-Concrete Beams Incorporating Recycled Utility Poles.” Thesis. Colorado State University. 2007.

5. LeBorgne, M. & Gutkowski, R.M. “Load Testing of Wood-Concrete Beams Incorporating Recycled Utility Poles,” Report No. 08-197, Mountain-Plains Consortium, North Dakota State University, Fargo, N.D; April 2008.

6. Fragiacomo, M. (2005). “A Finite Element Model for Long-Term Analysis of Timber-Concrete Composite Beams.” Structural Engineering and Mechanics, Vol. 20. No. 2, pp. 173-189.

7. Fragiacomo, M., & Ceccotti, A. (2006). “Long-Term Behavior of Timber-Concrete Composite Beams. I: Finite Element Modeling and Validation.” *Journal of Structural Engineering*, Vol. 132, No. 1, pp. 13-22.

8. Pault, Jerrold. “Composite Action in Glulam Timeber Bridge Systems.” Thesis. Colorado State University. 1977.

9. Ceccotti, A. (2002). “Composite Concrete-Timber Structures.” *Progress in Structural Engineering and Materials*, Vol. 4, No. 3, pp. 264-275.

10. Natterer, J., Hamm, J., Favre, P. “Composite Wood-Concrete Floors in Multi-Story Buildings.” Proceedings of the International Wood Engineering Conference. New Orleans, Louisiana, October 28-31, 1996, pp. 3431-3435.

11. Gutkowski, R., Brown, K., Shigidi, A., Natterer, J. (2007) “Laboratory Tests of Composite Wood-Concrete Beams.” *Construction and Building Materials*. Vol. 22, No. 6, pp. 1059-1066.

12. Gutkowski, R., Balogh, J., Natterer, J., Brown, K., Koike, E., & Etournaud, P. 2000. “Laboratory Tests of Composite Wood-Concrete Beam and Floor Specimens.” Proceedings of the World Conference on Timber Engineering – 2000, Whistler Resort, B.C., Canada; Department of Civil Engineering, Department of Wood Science; School of Architecture, University of British Columbia, Vancouver, Canada.

13. Dias, AMPG, “Mechanical Behaviour of Timber-Concrete Joints.” Ph.D. Thesis, University of Coimbra, Portugal. 2005.

14. Brown, Kevin. “Testing of a Shear Key/Anchor in Layered Wood/Concrete Beams.” Thesis. Colorado State University, 1998.

15. Etournaud, Patrick. “Load Tests of Composite Wood-Concrete Deckings under Point Loads.” Thesis. Colorado State University, 1998.

16. Koike, Eric. “Analysis of Composite Wood-Concrete Layered Beams.” Thesis. Colorado State University, 1998.

17. To, Lam. “3D Finite Element Modleing of Time-Dependent Behavior of Composite Wood-Concrete Beams.” Dissertation. Colorado State University, 2009.

18. Amadio, C. & Fragiacomo, M. “A Finite Element Model for the Study of Creep and Shrinkage Effects in Composite Beams with Deformable Shear Connections.” *Construzioni Metalliche*, 4, 1993, pp. 213-228.

19. Balogh, J., Wieligmann, M., Gutkowski, R., & Haller, P. “Stress-Strain Behavior of Connections for Partially Composite Wood-Concrete Floors and Deck Systems,” Proceedings of the 2nd Material Spec. Conf. of the Canadian Soc. of Civil Eng., Montreal, Canada, 2002.

20. Kuhlmann, U. & Michelfelder, B. “Grooves as Shear Connectors in Timber-Concrete Composite Structures.” Proceedings of the 8th World Conference on Timber Engineering, WCTE 2004. Lahti, Finland. June 14-17, 2004. Vol. 1. pp. 301-306.

21. LeBorgne, M. and Gutkowski, R. M., “Effects of Various Admixtures and Shear Keys in Wood-Concrete Composite Beams”. Submitted to *Construction and Building Materials*. Elsevier Publications. Edinburgh, Scotland.

22. Fritz-Pak Concrete Admixture. “Supercizer 7 High Performance Super Plasticizer.” 2005. 16 January 2009 <http://www.fritzpak.com/pdfs/pb115_supercizer7.pdf>

23. American Forest & Paper Association. National Design Specification for Wood Construction. (2005).

24. American Concrete Institute. 318-05: Building Code Requirements for Structural Concrete and Commentary. 2005.

25. Hanhijärvi, A. “Deformation Kinetics Based Rheological Model for the Time-Dependent and Moisture Induced Deformation of Wood.” *Wood Science and Technology*. Vol. 29, No. 3, 1995, pp. 191-200.

26. Neville, A.M. “Creep of Concrete: Plain, Reinforced, and Prestressed.” North-Holland Publishing Company. Amsterdam. 1970.

27. ACI Committee 209. “Prediction of Creep, Shrinkage, and Temperature Effects in Concrete Structures, (ACI 209-82),” American Concrete Institute. 1982.

28. CEB-FIP Model Code for Concrete Structures 1990, “Evaluation of the Time Dependent Behaviour of Concrete,” *Bulletin d’Infromation* No. 199, Comite European du Béton/Fédération Internationale de la Precontrainte, Lausanne, 1991.

29. Gardner, N.J. & Zhao, J.W. “Creep and Shrinkage Revisited.” *ACI Materials Journal*. Vol. 90, No. 3, 1993, pp. 236-246.

30. Goel, R., Kumar, R., Paul, D.K. "Comparative Study of Various Creep and Shrinkage Prediction Models for Concrete." *Journal of Materials in Civil Engineering*, Vol. 19, No. 3, March 2007, pp. 249-260.

31. Gardner, N.J. & Lockman, M.J. "Design Provisions for Drying Shrinkage and Creep and Normal-Strength Concrete." *ACI Materials Journal*. Vol. 98, No. 2, 2001, pp. 159-167.

32. Zhuoping, S. "The Variable Parameter Rheological Model of Wood." *Wood Science and Technology*. Vol. 39, No. 1, 2005, pp. 19-26.

33. Fragiacomo, M., Gutkowski, R. M., Balogh, J., & Fast, R.S. (2007). "Long-Term Behavior of Wood-Concrete Composite Floor/Deck Systems with Shear Key Connection Detail." *Journal of Structural Engineering*, ASCE, Vol. 133, No. 9, pp. 1307-1315.

34. ASTM C192-98. Standard Practice for Making and Curing Concrete Test Specimens in the Laboratory. "ASTM Standards in ACI 301 and 318." American Society of Testing and Materials. 1999.

35. ASTM C39-96. Standard Test Method for Compressive Strength of Cylindrical Concrete Specimens. "ASTM Standards in ACI 301 and 318." American Society of Testing and Materials. 1999.

36. Ducret, J.M. & Lebet, J.P. "Behaviour of Composite Bridges during Construction." *Structural Engineering International*, IASBE, Vol. 9, No. 3, 1999, pp. 212-218.

37. Fragiacomo, M., (2006). "Long-Term Behavior of Timber-Concrete Composite Beams. II: Numerical Analysis and Simplified Method." *Journal of Structural Engineering*, Vol. 132, No. 1, pp. 23-33.

38. Miller, Nathan. "Long-Term and Repeated Load Behavior of Wood-Concrete Composite Beams Incorporating Utility Poles." Thesis. Colorado State University, 2009.

39. Libby, J. R. Modern Prestressed Concrete. 2nd Edition. 1977

8. APPENDIX A. EXAMPLE DESIGN PROGRAM (SPECIMEN M2)

Composite Telephone Pole

INPUT: Ponderosa Pine

Material Properties

MOE Wood	Ew=	1.238E+06 psi	Density of Concrete=ρ=	0.150 kips/ft^3			
Mosture Content=m.c.=		8 %	f'c=	6890 psi	actual f'c=	psi	
Specific Gravity of Wood=G=		0.5					

Crossectional Dimensions of the Concrete

hc=	6.5 in	depth to transverse reinforcement=dt=	3.25 in				
wc=	23.5 in						

Cross Sectional Dimensions of the Wood

dw @ cL=	11.345 in			Fb Clear Wood=	5505.618		
				Ft Clear Wood=	3028.09		

Length of Beam

L=	24.58333333 ft						

Notch Dimensions

				Height of Dowel Washer in Conc=hwc.=	1 in		
height=hn=	3 in	Length from end to notch 1=Ln1=	28 in	Dowel Dia=dd=	0.625 in	fy-dowel=	36000 psi
Angle=θn=	10 deg	Length from end to notch 2=Ln2=	61.00 in	lth of Bearing Plate on Wood=wb=	4 in	notch hbn=	0.5 in
Notch Width=/ n=	9 in	Length from end to notch 3=Ln3=	123.00 in	Dia of Dowel Washer in Conc.=	2.25 in		

NDS Values

Fb=	1000 psi	Ccs=	1	Cf tension=	1	Kf-Fb,Ft,Fv,Fc,Frt,Fs=	2.16
Ft=	675 psi	Cm=	1	Cf comp=	1	Kf-Fc$^{\perp}$=	1.875
Fv=	90 psi	Ct=	1	Cfu=	1	λ=	0.8
Fc$^{\perp}$=	320 psi	Cl=	1	Ci=	1	Dead Factor=	1.2
Fc=	650 psi	Cf bending=	1	Cr=	1	Live Factor=	1.6

Steel Reinforement

Asb=	0.11 in^2 / bar	fy=	60000 psi

Slip Modulus

Kmid=	1.45990E+06 lbs/in
Knotch=	5.88612E+06 lbs/in

CALCULATIONS FULLY COMPOSITE:

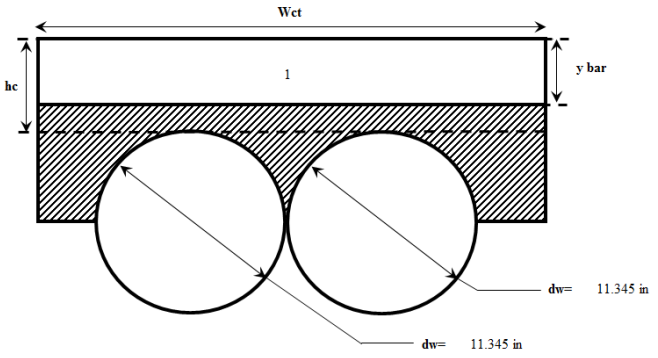

Transformed Concrete Width

Ec=	3.83E+06 psi
Ew=	1.2380E+06 psi
n=	3.0905
Wct=	72.63 in

Neutral Axis Location of Transformed Section from Top

y bar=	5.906 in	Neutral Axis is in the Concrete

Transformed Concrete Area

Act=	428.97 in^2

Moment due to Dead Load

ρw=	0.03253 kips/ft^3
Ac=	184.97 in^2
Aw=	202.18 in^2
wdead=	0.2860 kips/ft
Mdead@cL=	259.27 kip-in

Moment of Inertia of Transformed Section at Mid Span

Aw/2=	101.0878318 in^2
I1=	4,988.36 in^4
I2=	4782.26 in^4
I3=	4782.26 in^4
I bar=	14,552.87 in^4

Bending and Axial Limits for the Wood

F't=	1166.4 psi
Fb*=	1728.0 psi
Fb**=	1728.0 psi

ybar at Inner Notch

wnt=	10.0070 in
wnb=	4.6573 in
weq=	4.6597 in
heq=	7.8450 in
ybar-inner=	5.6091 in

Moment of Inertia at Inner Notch

Iceq=	4272.25 in^4
Iweq=	9386.47 in^4
Ibar-inner=	13658.72 in^4

Max Tension at Inner Notch Check

Ibar-inner=	13,659 in^4	
ybar-inner=	5.609 in	
Notch length=	9 in	
a=	127.50 in	
r=	5.6725 in	
A-skey=	42.77 in^2	
A-bkey=	3.1333 in^2	
A-dowel=	10.79 in^2	
A-gross wood=	202.18 in^2	
A-net=	145.48 in^2	

Allowable Three Point Bending Load for a Fully Composite Beam

Mmax=	1515.17 kip-in	1681.47 kip-in
Mu=	1255.90 kip-in	1422.21 kip-in
Pu=	17.029 kips	19.284 kips

Stress Calculations

fw*=	1.2430 ksi	
fw**=	0.0618 ksi	
ftw=	0.6524 ksi	
fbw=	0.5906 ksi	
ftw/F't+fbw/Fb*=	0.9011 ≤1	Bending to Tension Ratio OK
(fbw-ftw)/Fb**=	-0.0358 ≤1	Bending to Tension Ratio OK
fc*=	-1.9005 ksi	
fcc=	-0.9503 ksi	
fbc=	-0.9503 ksi	

Tension and Compression in the Wood and Concrete

Tw=	131.90 kips	
Cc=	-131.90 kips	

Concrete Strain Limit at cL

Єc max=	0.0030000	
Єc actual=	0.0004967	Concrete Strain Limit OK

Moment at Inner Notch

M inner=	1340.11 kip-in	

Stresses at Inner Notch

fw*=	1.1515 ksi	
fw**=	0.3818 ksi	
ftw=	0.7666 ksi	
fbw=	0.3849 ksi	
fc*=	-1.7008 ksi	
fcc=	-0.8504 ksi	
fbc=	-0.8504 ksi	
ftw/F't+fbw/Fb*=	1.000 ≤1	Bending to Tension Ratio OK
(fbw-ftw)/Fb**=	-0.30 ≤1	Bending to Tension Ratio OK

Horizontal Shear

Q=	1,266.85 in^3	
V-Notch 1=	11.363 kips	11.36274348
V-Notch 2=	10.576 kips	
V-Notch 3=	9.099 kips	
q-1=	0.9891 kips/in	
q-2=	0.9207 kips/in	
q-3=	0.7920 kips/in	
Vh-Notch 1=	44.017 kips	
Vh-Notch 2=	43.732 kips	131.71
Vh-Notch 3=	43.958 kips	

Notch Bearing Force

Fb-1=	44.696 kips
Fb-2=	44.407 kips
Fb-3=	44.636 kips

Stress at Center Line Fully Composite (ksi)

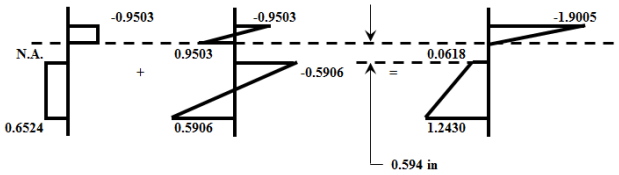

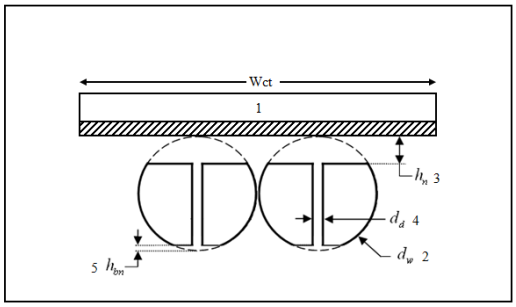

Stress at Inner Notch for Fully Composite (ksi)

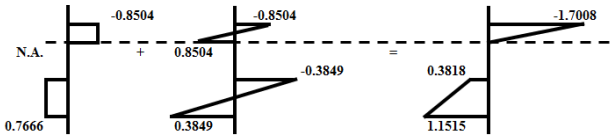

Stress at Inner Notch Adjusted for Horizontal Shear (ksi)

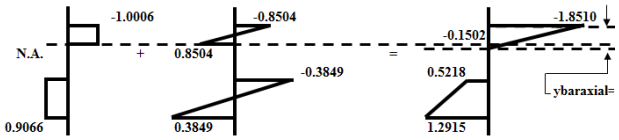

Service Load=Pa= 10.643 kips

Wood Horizontal Shear

Vwh-1=	44.017 kips	
Vwh-2=	43.732 kips	
Vwh-3=	43.958 kips	

Horizontal Shear in Wood Check

F'v=	155.52 psi	
w-shear=	20.01 in	
f-vh-1=	78.55 psi	Distance From End to Notch 1 OK
f-vh-2=	91.04 psi	Distance From End to Notch 2 OK
f-vh-3=	41.44 psi	Distance From End to Notch 3 OK

Wood Vertical Shear from Notch Interface

Vwv-1=	7.761 kips
Vwv-2=	7.711 kips
Vwv-3=	7.751 kips

Vertical Shear in Wood Check

F'v=	155.52 psi	
ybar-support=	2.407 in	
A-support=	50.54 in^2	
Q-support=	121.7 in^3	
I-support=	813.2 in^4	
fv-support=	131.17 psi	Shear at Support OK
Anet=	145.48 in^2	
ybar-notch=	7.358 in	
Q-notch=	121.68 in^3	
fv-notch 1=	51.19 psi	Shear at Notch 1 OK
fv-notch 2=	3.03 psi	Shear at Notch 2 OK
fv-notch 3=	3.04 psi	Shear at Notch 3 OK

Bearing Strength of Notch Check (notch height)

A-key=	42.77 in^2	
F*c=	1123.2 psi	
lb=	5.290E-01 in	
Cb=	1.7089	
F'c⊥=	820.3 psi	
F'θ=	1110.8 psi	
f-bearing-1=	1044.9 psi	Bearing at Notch 1 OK
f-bearing-2=	1038.2 psi	Bearing at Notch 2 OK
f-bearing-3=	1043.6 psi	Bearing at Notch 3 OK

Bearing Strength of Dowel Check

Cb=	1.094	
F'c⊥=	525.0 psi	
A-bearing=	15.693 in^2	
f'c⊥-1=	247.3 psi	Bearing at Dowel Washer 1 OK
f'c⊥-2=	245.7 psi	Bearing at Dowel Washer 2 OK
f'c⊥-3=	247.0 psi	Bearing at Dowel Washer 3 OK

Bearing Strength of Concrete Check

A-key=	42.773 in^2	
σbn=	3,806.7 psi	
σ-bc1=	1,044.9 psi	Bearing on Concrete 1 OK
σ-bc2=	1,038.2 psi	Bearing on Concrete 2 OK
σ-bc3=	1,043.6 psi	Bearing on Concrete 3 OK

Concrete Vertical Shear

Agv=	223.25 in^2	
Vcn*φ=	46.137 kips	
Vu-cv-1=	7.761 kips	Vertical Shear Notch 1 OK
Vu-cv-2=	7.711 kips	Vertical Shear Notch 2 OK
Vu-cv-3=	7.751 kips	Vertical Shear Notch 3 OK

Concrete Horizontal Shear Capactiy

Ac=	211.50 in^2	
Avf=	0.4970 in^2	
Vcn*φ=	74.185 kips	
Vu-ch-1=	44.017 kips	Horizontal Shear Notch 1 OK
Vu-ch-2=	43.732 kips	Horizontal Shear Notch 2 OK
Vu-ch-3=	43.958 kips	Horizontal Shear Notch 3 OK

Bearing on Concrete from Dowel Check

A1=	3.669 in^2	
d2=	11.345 in	
A2=	100.78 in^2	
Fbn*φ=	27.936 kips	
Fbu-1	3.8807 kips	Bearing on Concrete From Dowel 1 OK
Fbu-2	3.8556 kips	Bearing on Concrete From Dowel 2 OK
Fbu-3	3.8755 kips	Bearing on Concrete From Dowel 3 OK

20.951
27.337

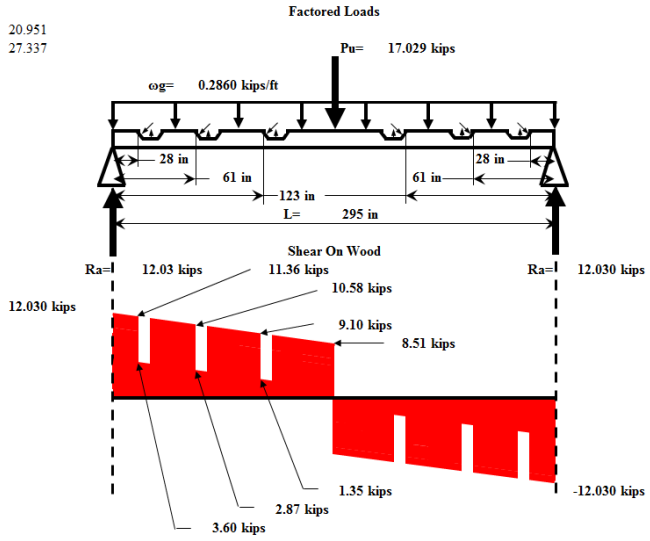

Mmax-composite= 1515.17 kip-in

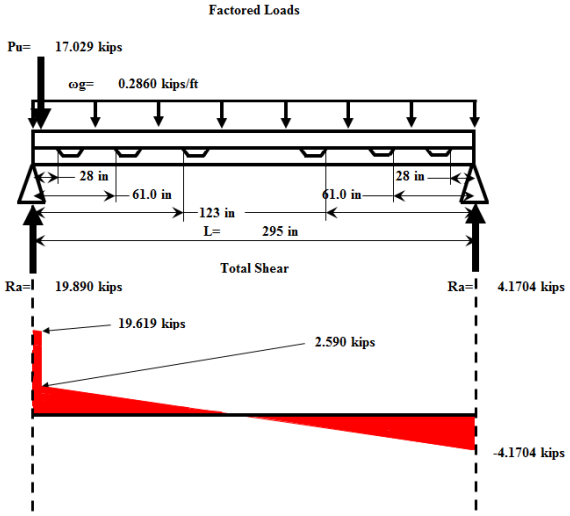

Mmax-composite= 1515.2 kip-in

Initial Deflection From Concrete

wc=	16.056 lbs/in
Iw=	1626.36 in^4
Delta D=	0.7864 in

Deflection Fully Composite

L=	295 in
wg=	23.83 lbs/in
Pu=	10660 lbs
Ew=	1.24E+06 psi
I-bar=	14,552.87 in^4
Delta L=	0.3165 in
Delta L+D=	0.4469 in

3.026715024

Deflection Not Composite

I-concrete=	1662.12 in^4
I-wood=	1626.36 in^4
I-total=	3288.48 in^4
Delta L=	1.4004 in
Delta D=	0.5773 in
Delta L+D=	1.9777 in

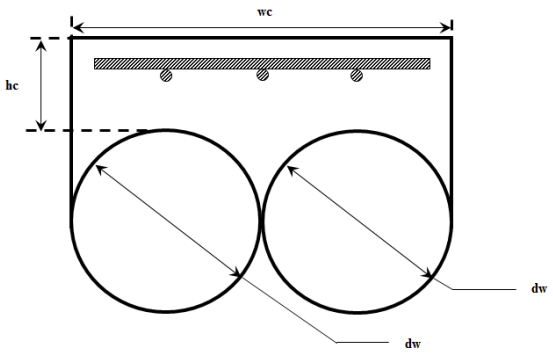

Transverse Reinforcement for Strength

ha=	4.0111 in
wa=	4.0111 in
wcL=	0.7246 kips/in
d-transverse=	3.25 in
Ts-transverse=	1.500 kips/ft
Strength #Bars=	0.227 bars/ft
Min #Bars=	1.276 bars/ft
Req #Bars=	1.276 bars/ft
Req Spacing=	9.40 in

Minimum Longitudinal Reinforcement

Min #Bars=	4.0 bars

12 inch splice

Required Volume of Concrete

Volume=	1.170 yds^3

Creep Prediction

Time=	28 days
Delta creep=	0.639 in
Delta total=	1.4259 in